Mohamed Khider University of Biskra
Faculty of exact sciences and Natural and life sciences
Material sciences department

MASTER MEMORY

Material Sciences

Physics

Energetic Physics and Renewable Energies

Ref:

Presented by:

Gana Noura

Le: 18/6/2023

Study of different graphene-based heterojunction solar cells by simulation

---

Jury:

M^{me}	Ouamane Samia	MCB	Mohamed Khider University of Biskra	President
M^{r}	Boumaraf Rami	MCB	Mohamed Khider University of Biskra	Supervisor
M^{me}	Messei Nadia	MCB	Mohamed Khider University of Biskra	Examiner

Academic Year: 2022/2023

ACKNOWLEDGEMENT

First, I would like to express my deep and sincere gratitude to my research supervisor Dr.Boumaraf Rami.

I would not forget to thank the members of the jury, Ouamane Samia and Messei Nadia who have kindly accepted to read and examine our work.

Words cannot express my gratitude to my mother and my siblings for the constant support that they have been for me.

Finally, I am also thankful to my best friend and other friends for supporting me.

Noura Gana

SUMMARY

Since applying graphene to silicon solar cells in 2010, researchers carrying out several researches to study the effect of graphene on the electrical characteristics and physical parameters of different solar cells. In this work, we have used SILVACO ATLAS simulation software to compare different graphene solar cells such as Gr/Si, Gr/GaAs and Gr/InP and simulate the effect of various physical parameters such as thickness and work function on the electrical properties of each solar cell, J_{SC} (short-circuit current density), V_{OC} (circuit voltage Open), FF (Fill Factor), η (efficiency), where this simulation was performed under AM1.5 irradiation. The results show that the best cell was InP with conversion efficiency of 8.02%.

Keywords : Graphene, solar cells, simulation, Silvaco.

RESUME

Depuis l'application du graphène aux cellules solaires au silicium en 2010, les chercheurs ont mené plusieurs recherches pour étudier l'effet du graphène sur les caractéristiques électriques et les paramètres physiques de différentes cellules solaires. Dans ce travail, nous avons utilisé la simulation du logiciel SILVACO ATLAS pour comparer différentes cellules solaires au graphène (comme Gr/Si, Gr/GaAs and Gr/InP) et simuler l'effet de divers paramètres physiques tels que l'épaisseur et la fonction de travail sur les propriétés électriques de chaque cellule solaire, J_{SC} (densité de courant de court-circuit), V_{OC} (circuit voltage Open), FF (Fill Factor), η (efficacité), où cette simulation a été réalisée sous irradiation AM1.5. Les résultats montrent que la meilleure cellule c'est celle de l'InP ou l'efficacité atteindre 8.02%.

Mots-clés : Graphene, cellules solaires, simulation, Silvaco.

ملخص

منذ تطبيق الغرافين على الخلايا الشمسية السيليكونية في عام 2010، أجرى الباحثون العديد من الأبحاث لدراسة تأثير الغرافين على الخصائص الكهربائية والفيزيائية للخلايا الشمسية المختلفة. في هذا العمل، استخدمنا المحاكاة بواسطة برنامج سلفاكو أطلس لمقارنة خلايا الغرافين الشمسية المختلفة (مثل Gr/Si, Gr/GaAs and Gr/InP) ومحاكاة تأثير المعلمات الفيزيائية المختلفة مثل السمك ودالة العمل على الخصائص الكهربائية لكل خلية شمسية، J_{SC} (كثافة تيار الدارة القصيرة) ، V_{OC} (جهد الدارة المفتوحة)، FF (معامل التعبئة) η (الكفاءة)، حيث تم إجراء هذه المحاكاة تحت إشعاع AM1.5. بينت النتائج أن أحسن خلية شمسية كانت المصنوعة من InP حيث بلغت كفاءتها 8.02%.

كلمات مفتاحية: غرافين، خلايا شمسية، محاكاة، سيلفاكو.

TABLE OF CONTENTS

Chapter II: materials properties

Chapter III: simulation and results

LIST OF FIGURES

LIST OF TABLES

LIST OF SYMBOLS

λ	wavelength.
ν	frequency of the light wave.
h	Planck's constant.
E	energy of the photon.
C	the speed of light in a vacuum.
AM	Air Mass
SBH	The Schottky barrier height
ϕ_M	The work function of the metal
ϕ_S	The work function of the metal
V_{bi}	The potential barrier of Schottky
X	Affinity
q	the elementary charge
v	voltage
n	the ideality factor
K_B	the Boltzmann constant
T	the absolute temperature
w_n	is the width of the depletion region
q	is the absolute value of electron charge
I_{ph}	photo-generated current
I_{SC}	Short circuit current
V_{OC}	Open-circuit voltage
J	Current Density
E_g	Energie de gap
FF	Fill Factor
Η	Efficiency
QE	Quantum Efficiency

EQE	External Quantum Efficiency
IQE	Internal Quantum Efficiency
SR	Spectral Response
R_S	the series resistance
R_{Sh}	is the shunt resistance
CdTe	Cadmium Telluride
CIGS	Copper-Indium-Gallium-Selenide
CVD	Chemical vapor deposition
Si	Silicon
GaAs	Gallium-Arsenide
InP	Indium-Phosphide
ε	The permittivity

Introduction

Introduction

The global energy consumption

Year after year, global energy consumption is rising continuously as shown in figure 1. This increased consumption is accompanied by increasing carbon dioxide (CO2) emitted from fossil fuels (gas, oil, coal) which is the bigger and more important source of generated global energy, the increasing rate of (CO2) is a cause of change climate and pollutes the environment [1]. But in the world energy outlook, the energy reserves of this source are limited, as indicated in figure 2. So renewable energy is the best substitute.

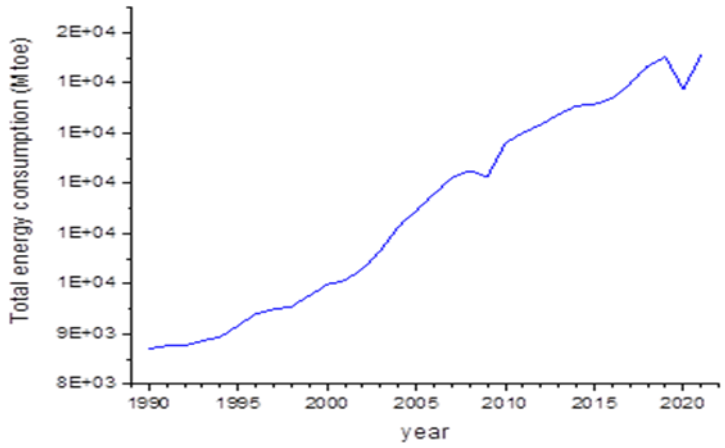

Figure 1: total energy consumption in the world (1990-2021) [2].

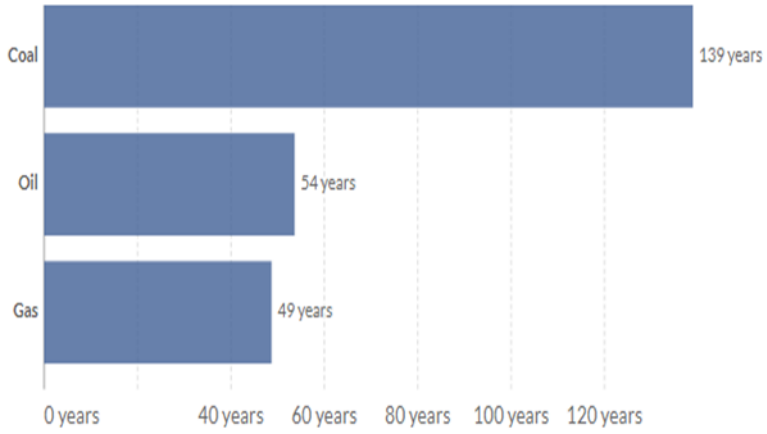

Figure 2: years of fossil fuel reserves left, 2020 [3].

The renewable energy

Renewable energy or clean energy is the best solution for producing energy without the dangers of climate change or the fear from runs out. For this, the production of electricity from renewable energy sources increased (almost 5% from 2020 to 2021), whereas in only the EU the share of renewable energy sources in gross electricity consumption increased from 37.4% in 2020 to 37.5% in 2021. The figure 3 indicated electricity consumption by renewable sources, where solar is the third important source after the wind and hydro. Solar power is the energy source it is fastest-growing, where in 2008 it accounted percentage of 1% of the electricity consumed in the EU.

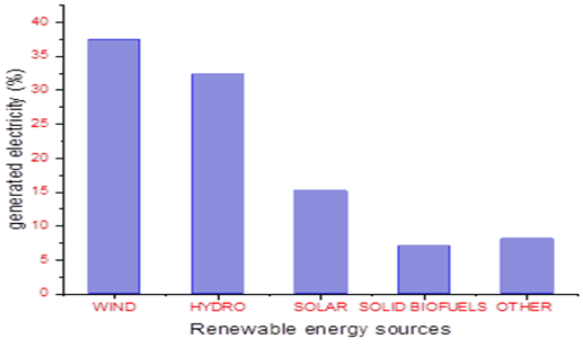

Figure 3: source of renewable energy in gross electricity consumption, EU, 2021 (%) [4].

Solar cells

When talking about the solar source that generated electricity, we mean solar cells, particularly PV solar cells. This source has witnessed continuous development and improvements over the years to improve efficiency. These improvements in used materials and methods of fabrication, Summarize and clarify all this in the four generations, as shown in figure 4. Among the improvements under study in used materials, it is used graphene material which is new material, and this is what we focus in this work.

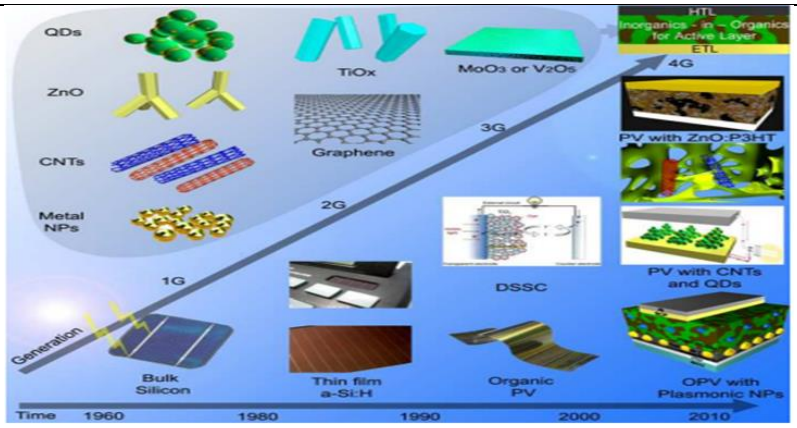

Figure 4: timeline of the four generations of photovoltaic devices, illustrating the changes from first generation (1G) to fourth generation (4G) with associated nanomaterial components that comprise half of the 4G devices [5].

In this work, we will compare different graphene-based heterojunction solar cells, by simulation using the Silvaco Atlas software.

This thesis contains three chapters:

- The first is an overview of solar cell principles with details.
- The second chapter describes details about the material properties which we using in our work.
- The third chapter is describing some definitions about SILVACO and analyzes the simulation results.

This work is complementary to previous studies[6, 7].

Chapter I

I.1 Introduction

Sunlight is the most important source of renewable energy specifically solar cells, this last are two forms: thermal converters which convert light into heat, and photovoltaic solar cells which convert the absorbed sunlight into electricity.

This chapter focuses on the fundamental concepts of photovoltaic solar cells (definitions, principles, characteristics, and types).

I.2 solar radiation

The Blackbody is a concept to define all objects that are good absorbers of radiation, which means, good absorbers of light. For we have learned that good absorbers are also good emitters. And some objects that are good absorbers of visible light also radiate in visible parts of the spectrum. Thus, black bodies don't always appear black (for instance the sun) [8].

The sun is a hot sphere of gas, the center of which is nuclear fusion reactions that heat it, as indicated in figure 1.1. Internal temperatures reach 20 million Kelvin, and the intense radiation from the interior is absorbed by a layer of hydrogen ions closer to the sun's surface. Energy is transferred by convection through this optical barrier and then re-radiated from the outer surface of the sun (the photosphere). The radiation emitted approximates that from a blackbody with a temperature of nearly 6000 K, as shown in figure 1.2 [9].

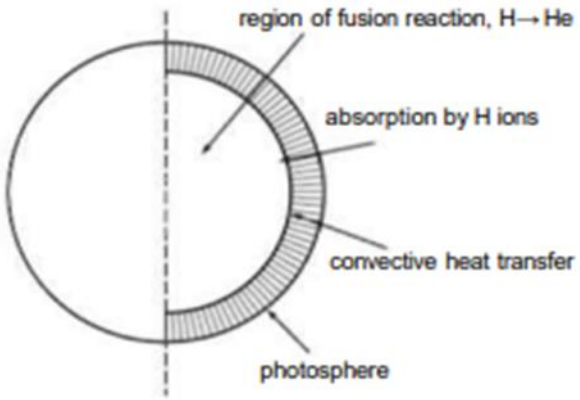

Figure 1.1: regions in the sun's interior [10].

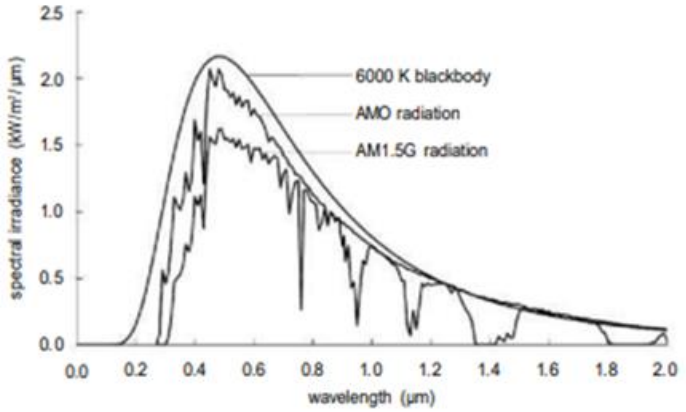

Figure 1.2: the spectral irradiance from a blackbody at 6000 compared with solar AM0 and AM1.5G spectra [10].

Sunlight is like any light, which is defined as a type of electromagnetic wave having a wave nature and also a particle nature. The first nature means that light moves in space while oscillating like a wave, and the second nature concerns the particle-like behavior that appears due to the quantization of the electromagnetic field. Therefore, it can be considered a wave or particle.

we call the particles photons When we treat the light in terms of particles. The energy of each single particle (photon) is proportional to the frequency of the photon, and the total power of some monochromatic light is proportional to the frequency of the photons and the number of photons.

From the previous definition, we can conclude two equations, the first one describes the relation between light energy (E) and light frequency (ν) and the second equation describes the relation between the frequency of the wave (ν), the propagation speed of the wave (c) and the wavelength (λ).

$$E = h\nu \qquad (1.1)$$

$$\nu = \frac{c}{\lambda} \qquad (1.2)$$

In equation 1.1 h is Planck's constant ($h \cong 4.14 \times 10^{-15} eV\ s$), and in equation 1.2 c is the speed of the wave equals the speed of light in vacuum $\left(c \cong 3.0 \times 10^{8} \frac{m}{s}\right)$ [11].

Although radiation from the sun's surface is constant, but when it reaches the earth surface it is highly variable due to absorption and scattering in the earth's atmosphere. When skies are clear, the maximum radiation strikes when the sun is vertical on the earth surface, and sunlight has the shortest pathlength through the atmosphere. Can calculate This

pathlength approximated by 1/cosφ. where φ is the angle between the sun and the point directly overhead, as shown in Figure 1.3. This pathlength is usually referred to as the Air Mass (AM) through which solar radiation must pass to reach the earth's surface. Then

$$AM = 1/cos\varphi \qquad (1.3)$$

When φ=0, the Air Mass equals 1 or 'AM1' radiation is being received; when φ=60°, the Air Mass equals 2 or 'AM2' conditions prevail. AM1.5 (equivalent to a sun angle of 48.2° from overhead) has become the standard for photovoltaic work [9].

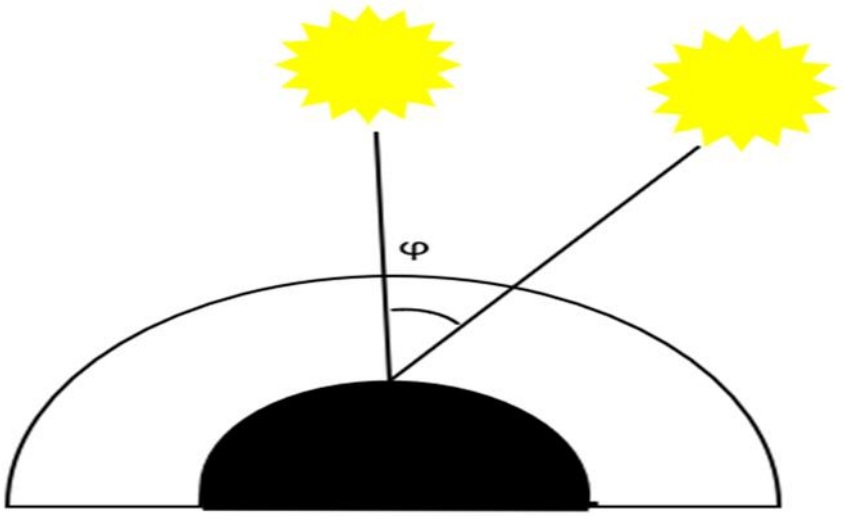

Figure 1.3: the sun position and pathlength of sunlight in atmosphere.

I.3 Solar cells

The photovoltaic solar cells are devices convert the solar radiation directly to electrical energy that madding from material which is able to convert the energy of light (photons) into electricity by using the photovoltaic effect [12]. So, the solar cell uses light-absorbing materials called semiconductor that generate pair from electron-hole when the material is illuminated. The process is called the excitation of charge carriers by light, resulting the electricity by separate the carriers to produce an external current through the load [13].

I.4 semiconductors

The materials can be divided into three types according to electricity conductivity: insulators, where no current that can be carried by electrons, their valence band is full and conduction band is empty, and have very high band gaps (band gap > 3eV). Conductors, are free to conduct electricity, their valence and the conduction bands overlap. Semiconductors, that have partially filled valence gaps over intermediate band gaps which have a band

structure like insulators but energy gap is much narrower (band gap < 3eV) and electrons of this materials can easily be excited by thermal or optical means.

In semiconductors, if the material that is doped has more electrons in its conduction band, so the semiconductor is called an n-type semiconductor. The n-type semiconductor is electronically neutral but has excess of electrons, which are available for conduction. On the other hand, if the material that is doped has fewer electrons in its valence gap so semiconductor is called a p-type semiconductor. The p-type semiconductor is electronically neutral but it has positive holes (missing electrons) in its structure, which can accommodate excess electrons. For example, silicon is semiconductor belongs to the 4th group of the periodic table of elements, if some Si atoms replaced with group 5 elements of periodic table, such as arsenic (As) or antimony (Sb), electrons will be freed can move around the crystal, in this case the silicon will be n-type, but when Si atoms replaced with group 3 elements of periodic table, such as gallium (Ga) or indium (In), free positive particles (the holes) will be formed that can move around the crystal through diffusion or drift, in this case the silicon will be p-type [14].

I.5 Schottky junction

Schottky junction (Schottky barrier) is created in metal-semiconductor (M-S) junction that can be found in every semiconductor device, all materials have a work function which is the energy difference between the Fermi level, and the vacuum level but in general the metal work function ϕ_M is different from the semiconductor work function ϕ_S, also the energy difference between the conduction band edge and the vacuum called electron affinity χ as shown in figure 1.4 [15].

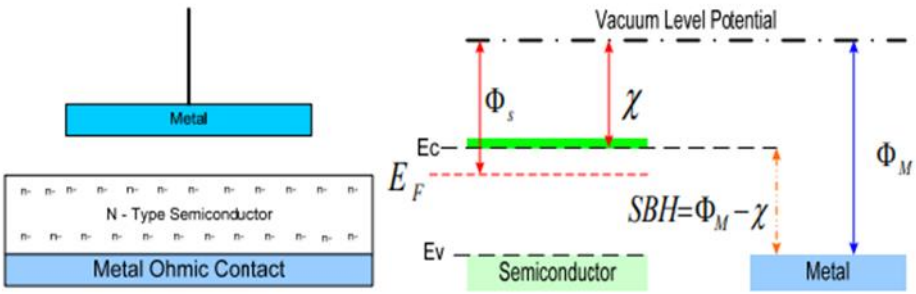

Figure 1.4: metal and semiconductor before contact; band diagram Schottky barrier height [16].

SBH: the Schottky barrier height.

The metal-semiconductor junctions can be divided into two type according to the value of metal and semiconductor work function: Schottky and ohmic.

- When $\phi_M > \phi_S$: The metal-semiconductor n-type junction is Schottky, the metal-semiconductor p-type junction is ohmic.
- When $\phi_M < \phi_S$: The metal-semiconductor n-type junction is ohmic, the metal-semiconductor p-type junction is Schottky [17].

When the metal makes contact with the semiconductor, in thermal equilibrium the Fermi levels must be equal in the two materials and the vacuum level must be continuous, as shown in figure 1.5, the Schottky barrier height ϕ_{Bn} (SBH) is the difference between the metal work function and the semiconductor electron affinity [15].

$$q\phi_{Bn} = q\phi_M - q\chi \qquad (1.4)$$

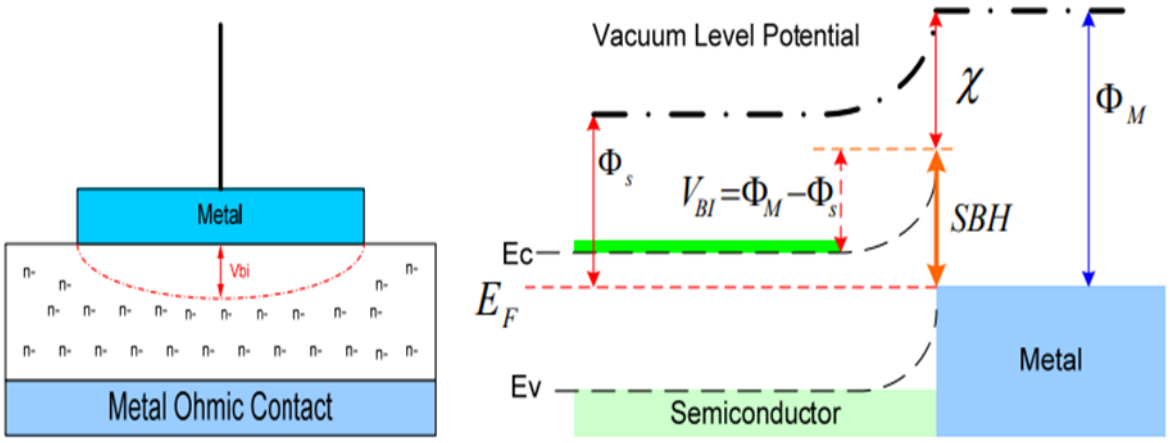

Figure 1.5: metal and semiconductor in contact; band diagram of built-in potential [16].

The equation (1.4) when is used in n-type semiconductor Schottky junction, but when the metal contact p-type semiconductor the barrier height $\phi_{Bp}$is given by [15]:

$$q\phi_{Bp} = E_g - (q\phi_M - q\chi) \qquad (1.5)$$

In figure 1.5, V_{BI} is the built-in potential (equilibrium contact potential) which is the mechanism that prevents any further charge movement from the semiconductor conduction band to the metal [16].

$$V_{BI} = \phi_M - \phi_S \qquad (1.6)$$

I.6 Principles of solar cell operation

The solar cell is an important candidate for a renewable energy source because they directly convert the sunlight into electricity using the photovoltaic effect after the absorption of light which generates an electron-hole pair. The electron and hole are separated by the structure of the device to the negative terminal (electron) and positive terminal (hole) thus generating electrical power[15, 18], as shown in figure 1.6. Solar cells are considered an important energy source, due to for several features:

- Good conversion efficiency.
- Provides nearly permanent power at a low operating cost.
- Virtually nonpolluting [15],

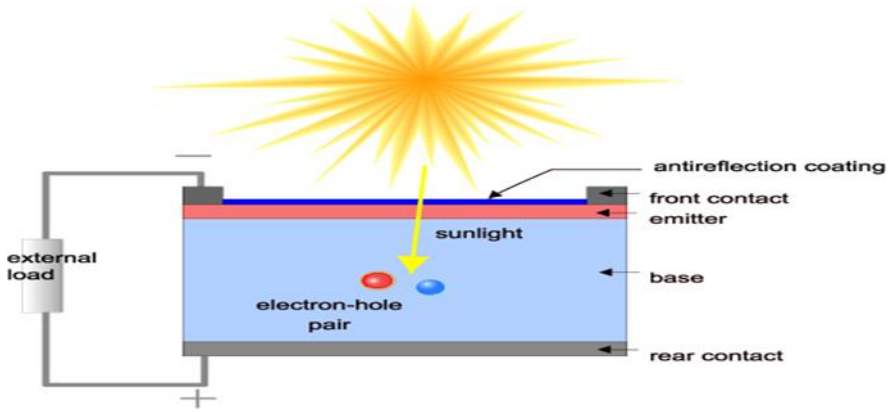

Figure 1.6: solar cell structure [19],

To find out the principles of solar cell operation have to know the solar cell structure first, which is made from two layers of semiconductor material, the first is from the n-type of semiconductor and the second p-type semiconductor, to shape p-n junction.

when p-n junction is created, majority carriers near the interface on both sides diffuse across the junction (electrons from the n-side and holes from the p-side) because of the difference in holes and electrons densities across the junction. Most of the electrons and holes which diffuse to the p-side and n-side, recombine with holes or electrons on each side. As a result, a region is formed near the junction that has been depleted of mobile carriers. An electric field exists in the depletion region separates any free electron-hole pairs that generate in this region. The p-n junction can be divided into three regions as seen in figure 1.7

1. The p-type region where the material is neutral and the bands are flat. The density of acceptors exactly balances the density of holes (assuming that all of the acceptors

are ionized). In general, the majority carriers (holes) density is equal to the density of ionized dopant.

2. The n-type region away from the junction where the material is neutral and the density of immobile donors exactly balances the free electron density (assume that all of the donors are ionized). In general, the majority carriers (electrons) density is equal to the density of ionized dopant.
3. Around the junction, there is a depletion region where the bands are bent and an electric field exists that sweeps the free carriers, leaving behind them positively charged donors in the n-region and negatively charged acceptors in the p-region. The depletion region extends along a distance of W_p in the p-region and a distance of W_n in the n-region [20].

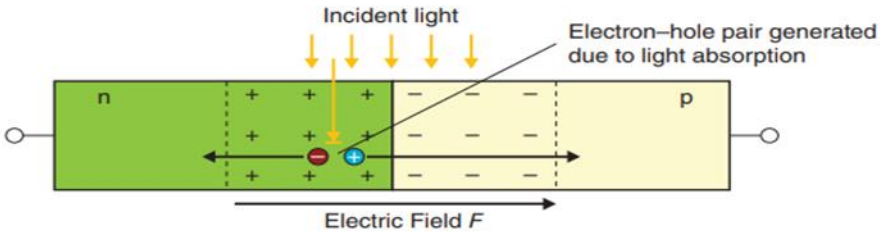

Figure 1.7: p–n junction [21].

From the p-n junction, can understand the principle of the solar cell in generating the current. [21]. But in Schottky junction solar cell is similar to one-sided the p-n junction, the width of depletion layer in a metal-semiconductor (n-type) contact can be expressed by [22]:

$$W_n = \sqrt{\frac{2\varepsilon_s}{qN_d}(V_{bi} - V - \frac{K_B T}{q})} \qquad (1.7)$$

Where W_n is the depletion width, ε_s is the permittivity of semiconductor, K_B is Boltzmann constant and equal $1.38 \times 10^{-23}\, J/K$, $T(K)$ is Temperature, and N_d is doping concentration.

I.7 Solar cell characteristics

An ideal solar cell can be represented by a current source connected in parallel with a rectifying diode, as shown in the equivalent circuit of figure 1.8. The corresponding I-V characteristic is described by the Shockley solar cell equation [23].

$$I = I_{Ph} - I_S(e^{\frac{qV}{K_B T}} - 1) \qquad (1.8)$$

Where: $I_{Ph}(A)$ is photo-generated current by the solar generator under illumination, $I_S(A)$ is saturation current of the solar cell, and $q(C)$ is Electric charge.

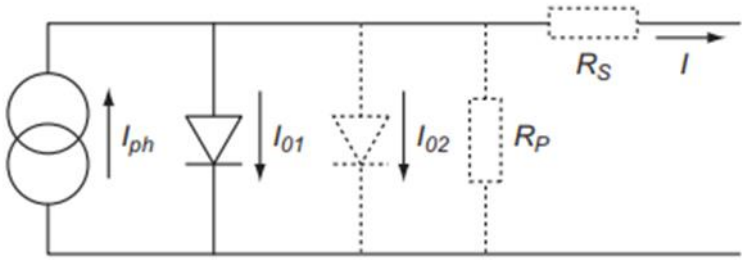

Figure 1.8: the equivalent circuit of an ideal solar cell (full lines). Non-ideal components are shown by the dotted line [18].

The I-V characteristic as shown in figure 1.9, is an important characteristic for extracting the other characteristics of solar cell.

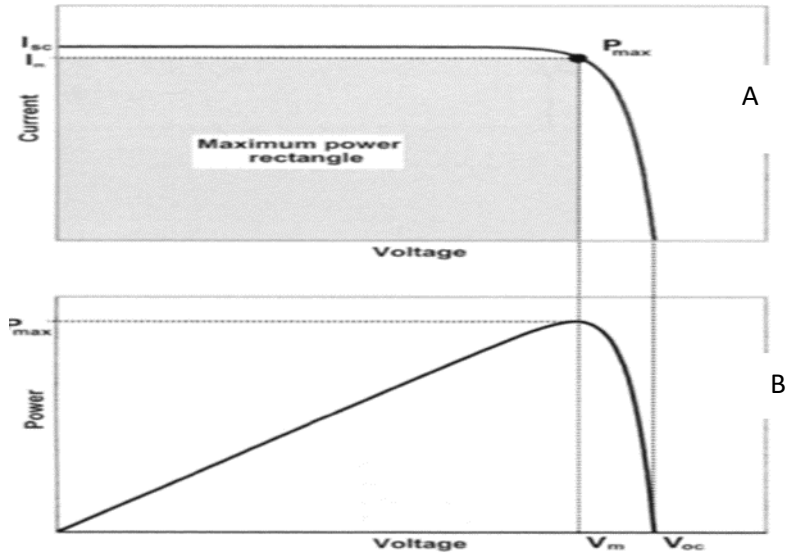

Figure 1.9: The I-V characteristic of an ideal solar cell (A) and the power produced by the cell. (B) The power generated at the maximum power point is equal to the shaded rectangle in (A) [23].

I.7.1 Short circuit current I_{SC}

The short-circuit current I_{SC} is the first value that can be calculated from the I-V characteristic, it is delivered by the solar cells when it is short-circuited at its connections; the voltage V is thus 0 [21].

$$I_{SC} = I(V = 0) = I_{Ph} - I_S(e^0 - 1) = I_{Ph} \qquad (1.9)$$

I.7.2 Open circuit voltage V_{OC}

The Open circuit voltage V_{OC} is the second value that can be calculated from the I-V characteristic, it is the bias value when the current becomes zero.[21] The open-circuit voltage is determined by equation (1.10) [23].

$$V_{OC} = \frac{K_B T}{q} \ln\left(\frac{I_{SC}}{I_S} + 1\right) \qquad (1.10)$$

Equation (1.10) expresses V_{OC} in p-n junctions, but in Schottky junction the current density is similar to the transport equation for p-n junctions. However, the expressions for the saturation current densities are quite different [22].

$$J = \left[A^{**}T^2 \exp\left(\frac{-q\phi_{Bn}}{KT}\right)\right]\left[\exp\left(\frac{qV}{KT}\right) - 1\right] \qquad (1.11)$$

When J is current density and $A^{**} = \frac{f_p f_Q A^*}{1+(f_p f_Q \upsilon_R/\upsilon_D)}$ (with is the effective Richardson constant for thermionic emission, $f_p$the probability of electron emission over the potential maximum, f_Q is the ratio of the total current flow, υ_D is integral of Dawson, and υ_R recombination velocity).

From equation (1.11), V_{OC} in Schottky junction can be deduced by the equation (1.12):

$$V_{OC} = \phi_{Bn} + \frac{q}{KT} \ln\left(\frac{J}{A^{**}T^2}\right) \qquad (1.12)$$

I.7.3 Fill factor FF

The fill factor FF is a measure of the quality of a cell, and describes the relationship between power P_m (the maximum power produced by the cell at a voltage V_m and current I_m) and the product of the open-circuit voltage and short-circuit current.

$$FF = \frac{I_m V_m}{V_{OC} I_{SC}} = \frac{P_m}{V_{OC} I_{SC}} \qquad (1.13)$$

I.7.4 Efficiency η

The efficiency of a solar cell describes what proportion of the optical power P_{Opt} incident on the cell is output again as electrical energy P_m, expressed as a percentage.

$$\eta = \frac{P_m}{P_{Opt}} = \frac{P_m}{E.A} = \frac{FF.V_{OC}.I_{SC}}{E.A} \qquad (1.14)$$

where A is cell area and E is the incident solar radiation [21].

I.7.5 The quantum efficiency

The quantum efficiency (QE) of a solar cell is the ratio of the number of electrons in the external circuit and the number of incident photons of a given wavelength. Thus, can define external quantum efficiency EQE(λ) which account all photons impinging on the cell surface, and internal quantum efficiency IQE(λ) which considers only photons that are not reflected.[23] The QE corresponds to the spectral response (SR) determined by equation (1.15) [24].

$$SR(\lambda) = \frac{I_{SC}(\lambda)}{I_{light}(\lambda)} \qquad (1.15)$$

When I_{light} is the light intensity, the IQE can be derived as:

$$IQE = \frac{1}{1-R(\lambda)} . \frac{I_{SC}(\lambda)/_{e}}{I_{light}(\lambda)/_{(hc/\lambda)}} = \frac{1}{1-R(\lambda)} . \frac{hc}{e\lambda} . SR(\lambda) \qquad (1.16)$$

With R (λ) is the front surface reflectance by wavelength. The EQE can be defined by:

$$EQE(\lambda) = \frac{hc}{q\lambda} SR(\lambda) \qquad (1.17)$$

where h is constant of Planck, c is the light speed, q is the electronic charge, and λ is the wavelength [25], figure 1.10 shows a graph of EQE in some solar cells. The relation between EQE and IQE can be written as:

$$IQE(\lambda) = \frac{EQE(\lambda)}{Abs_{AL}(\lambda)} \qquad (1.18)$$

where AL stands for the active layer, and Abs_{AL} is the absorption in the active layer [26],

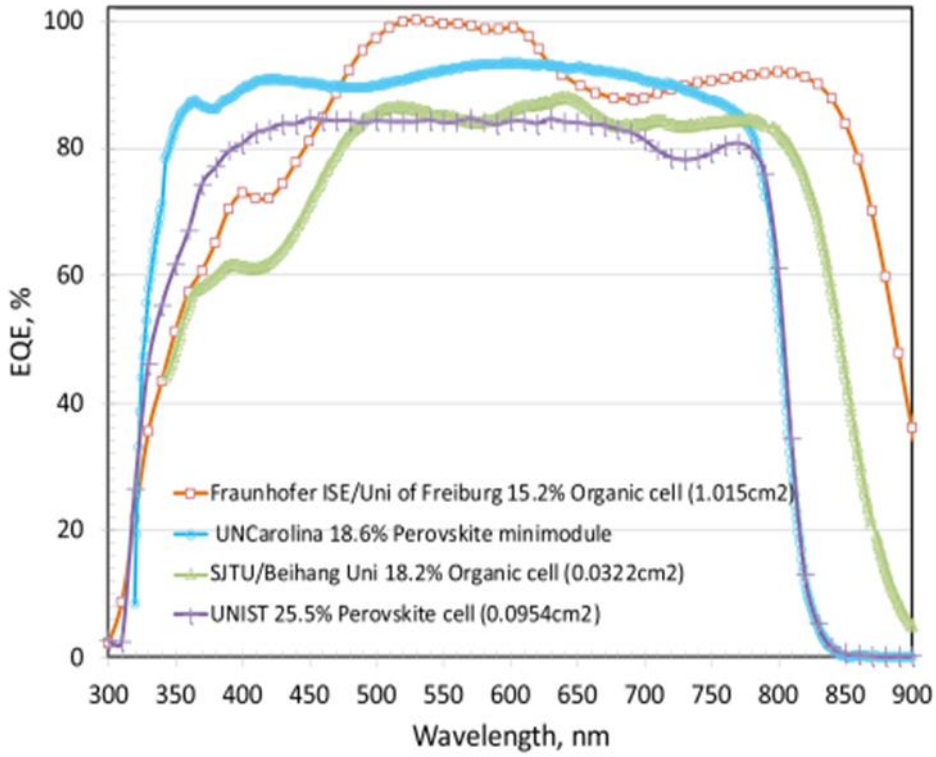

Figure 1.10: external quantum efficiency (EQE) for the new organic and perovskite cell and minimodule results (some results may be normalized) [27].

I.7.6 The series resistance

Series resistance R_S in a solar cell is a parasitic, power-consuming parameter that seriously affects the maximum conversion efficiency of an otherwise good cell [28], when taking the value of the series resistance into account, the current equation will be written as.

$$I = I_{Ph} - I_S(\exp\left(\frac{(V+IR_S)}{mK_BT/q}\right) - 1) \qquad (1.19)$$

Where m is quality factor [29].

I.7.7 The shunt resistance

The shunt resistance R_{Sh} or the leakage current resistance creates a parallel path of high conductivity in the solar photovoltaic panel, thus decreasing the output power and open circuit voltage [30]. In this condition current equation, is written as:

$$I = I_{Ph} - I_D - I_{Sh} \qquad (1.20)$$

When I_{Sh} is:

$$I_{Sh} = \frac{I_D}{R_{Sh}} = \frac{V+I.R_S}{R_{Sh}} \quad (1.21)$$

Therefore, the current equation becomes:

$$I = I_{Ph} - I_S\left(e^{\frac{V+IR_S}{m.V_T}} - 1\right) - \frac{V+I.R_S}{R_{Sh}} \quad (1.22)$$

Where $V_T = \frac{q}{K_B T}$

Equation (1.8) is Shockley solar cell equation in the condition of a simplified Model, but in some of other conditions the two-diode model is used instead, in which the diffusion current is modeled using a diode with an ideality factor of 1 and a recombination current through an additional diode with an ideality factor of 2, as shown in figure 1.11. The current equation will be [21]:

$$I = I_{Ph} - I_{S1}\left(e^{\frac{V+I.R_S}{V_T}} - 1\right) - I_{S2}\left(e^{\frac{V+I.R_S}{2V_T}} - 1\right) - \frac{V+I.R_S}{R_{Sh}} \quad (1.23)$$

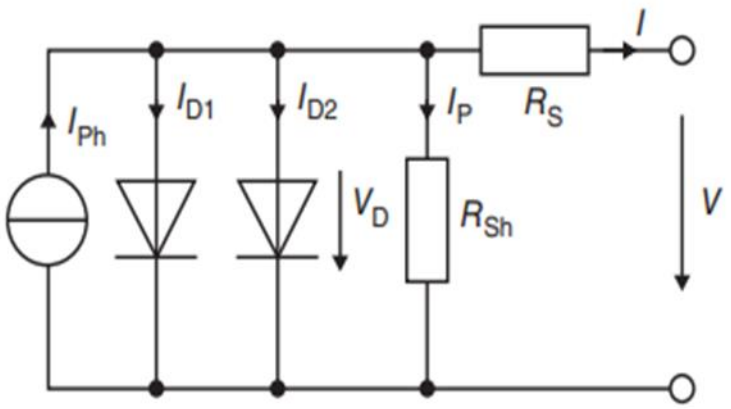

Figure 1.11: The two-diode model for possible exact modeling of the solar cell characteristic curve.

Figure 1.12 shows influence of series and shunt resistance on the solar cell characteristic curve in the two-diode model.

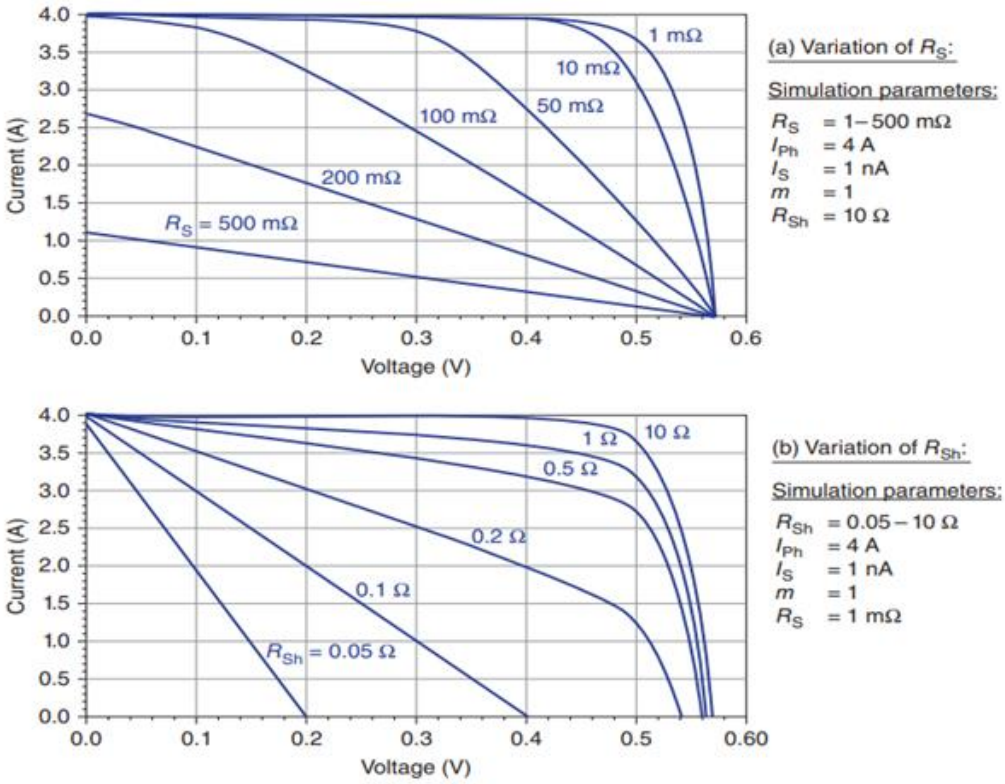

Figure 1.12: influence of series resistance, R_S(a), and shunt resistance, R_{Sh} (b), on the solar cell characteristic curve: The fill factor decreases significantly with an increase in RS and a decrease in R_{Sh} [21].

I.8 Types of solar cells

Solar cells are typically named after the semiconducting material they are made of. Solar cells can be classified into first, second, third and fourth generation cells [31].

I.8.1 First generation

The first-generation cells (traditional or wafer-based cells) are made of crystalline silicon, the technology of this type includes materials such as polysilicon and monocrystalline silicon, it is commercially dominant in PV technology [32].

I.8.1.1 Monocrystalline Solar Cells

Monocrystalline Cells are made of thin wafers of monocrystalline silicon which has a single continuous crystal lattice structure with almost no defects or impurities (thickness of about 200 μm) [33, 34]. But the disadvantage of these cells is that a complicated manufacturing process is required to produce monocrystalline silicon, which results in slightly higher costs than those of other technologies.[34] The estimated life span of these solar cells is around 25-30 years [33, 35].

I.8.1.2 Multicrystalline Solar Cells

Multicrystalline cells are made by using numerous grains of monocrystalline silicon. For the manufacturing process, molten polycrystalline silicon is cast into ingots, which are subsequently cut into very thin wafers and assembled into complete cells. These types of cells are cheaper to produce than monocrystalline cells [34].

I.8.2 second generation

Thin film solar cells are second-generation cells, which include amorphous silicon, CIGS, and CdTe cells, this type of solar cell is less expensive to produce than traditional silicon solar cells as they require less amount of construction materials

I.8.2.1 Amorphous silicon solar cells (A-Si)

Amorphous silicon panels are formed by vapor-depositing a thin layer of silicon (1µm) on a substrate material such as glass or metal. also, deposition on plastic can be done because Amorphous silicon can be deposited at very low temperatures (75 degrees Celsius). In its simplest form, the cell structure has a single sequence of p-i-n layers. However, single-layer cells suffer from significant degradation in their power output (in the range of 15-35%) when exposed to the sun. Better stability requires the use of thinner layers in order to increase the electric field strength across the material but this reduces light absorption, hence cell efficiency. This has led the industry to develop tandem and even triple layer devices that contain p-i-n cells stacked one on top of the other, as shown in figure 1.13 [32].

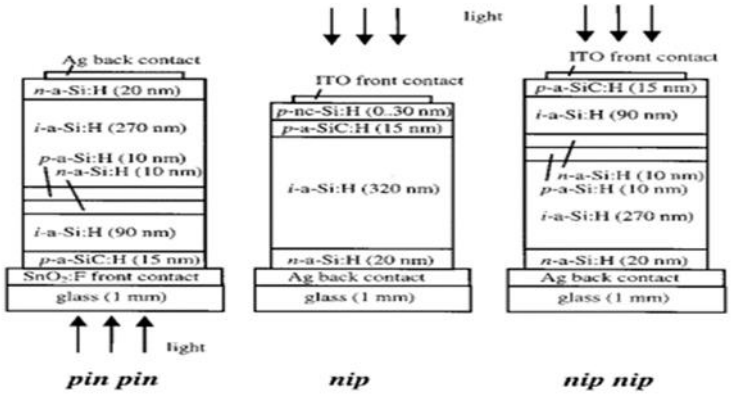

Figure 1.13: schematic device structures of pin pin, nip, and nip nip cells. The arrows indicate the incident light [36].

I.8.2.2 Cadmium telluride solar cell (CdTe)

Cadmium telluride (CdTe) has long been recognized as a strong candidate for thin solar cell applications. It has a bandgap of 1.45 eV, which is nearly ideal for photovoltaic energy conversion [37]. Cadmium telluride PV is the only thin film technology with lower costs than conventional solar cells made of crystalline silicon but there are limiting factors to the scalability of CdTe technology in the mid-term future the toxicity of cadmium (environmental concern), and the tellurium is a rare material. The figure 1.14 shown solar cell comprise CdTe.

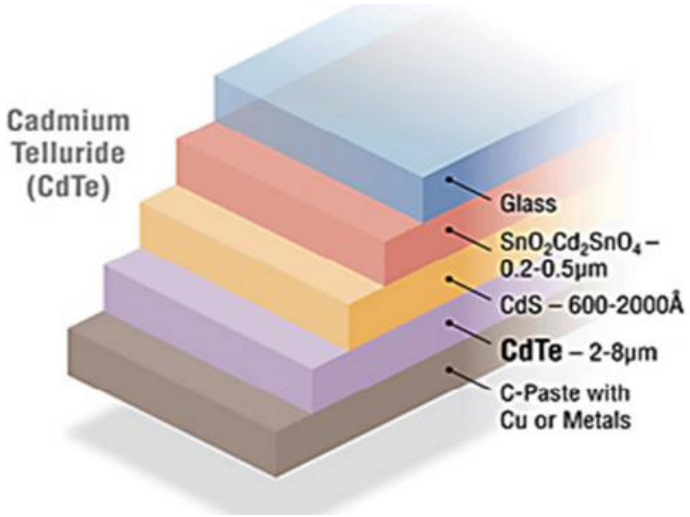

Figure 1.14: graphic showing CdTe solar cells.

I.8.2.4 Copper indium gallium selenide solar cells (CI (G) S)

A copper indium gallium selenide solar cell (CIGS) is a thin film PV solar cell. For manufacture, it deposits a thin layer of copper, indium, gallium, and selenide on glass or plastic backing, along with electrodes on the front and back to collect current. In CIGS a much thinner film is required than other semiconductor materials Because the material has a high absorption coefficient and strongly absorbs sunlight. The figure 1.15 shown solar cell comprise CIGS.

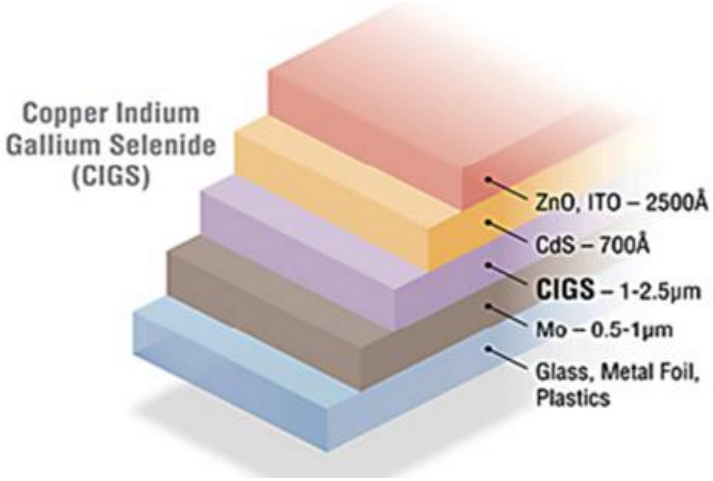

Figure 1.15: graphic showing CIGS solar cells.

I.8.3 Third generation

The third generation of solar cells includes several thin-film technologies. it is using organic materials, often organometallic compounds as well as inorganic substances. Even though their efficiencies had been low and the stability of the absorber material was often too short for commercial applications, its technologies are in invested research for achieve producing high-efficient, low-cost solar cells. Types of this generation:

I.8.3.1 Dye sensitized solar cells

Dye Sensitized solar cells (DSSC) were invented in 1991 by Professor Michael Graetzel and Dr. Brian, it is a new class of advanced solar cells that can be likened to artificial photosynthesis due to how it mimics the natural absorption of light energy. it belongs to the group of thin film solar cells and low-cost. It is based on a semiconductor formed between a photo-sensitized anode and an electrolyte, as shown in figure 1.16 [32].

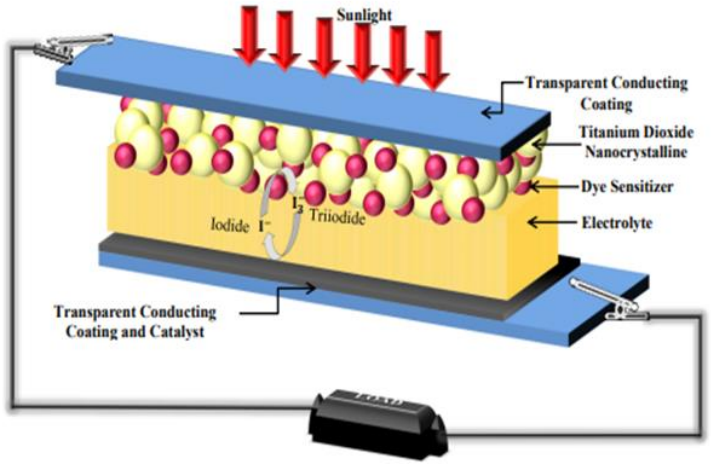

Figure 1.16: principle operation of dye-sensitized solar cells (DSSCs) [38].

I.8.3.2 Polymer solar cells

In polymer solar cells the material used to absorb the solar light is an organic material such as a conjugated polymer, it is a type of thin film solar cell, it is a flexible solar cell made with polymers (large molecules with repeating structural units), that generate electricity through the photovoltaic effect. Polymer solar cells are lightweight, inexpensive in fabrication, flexible, and potentially have a less adverse environmental impact. Figure 1.17 indicates the structure of the polymer solar cell and the molecular formula for polymers.

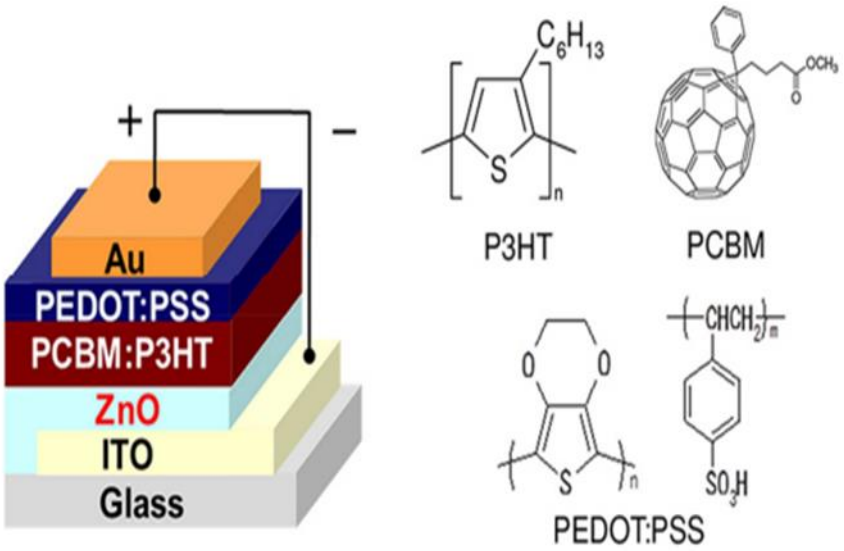

Figure 1.17: polymer solar cell and the molecular formula for polymers.

I.8.3.3 Quantum dot solar cells

Quantum dot solar cell is a solar cell design that uses quantum dots (semiconducting particles that have a small size) as the absorbing photovoltaic material. Quantum dots have bandgaps that are tunable across a wide range of energy levels by changing the size of dots, this is why is attractive for multi junction solar cells, the structure and operating principle of quantum dots solar cell is shown in figure 1.18 [32].

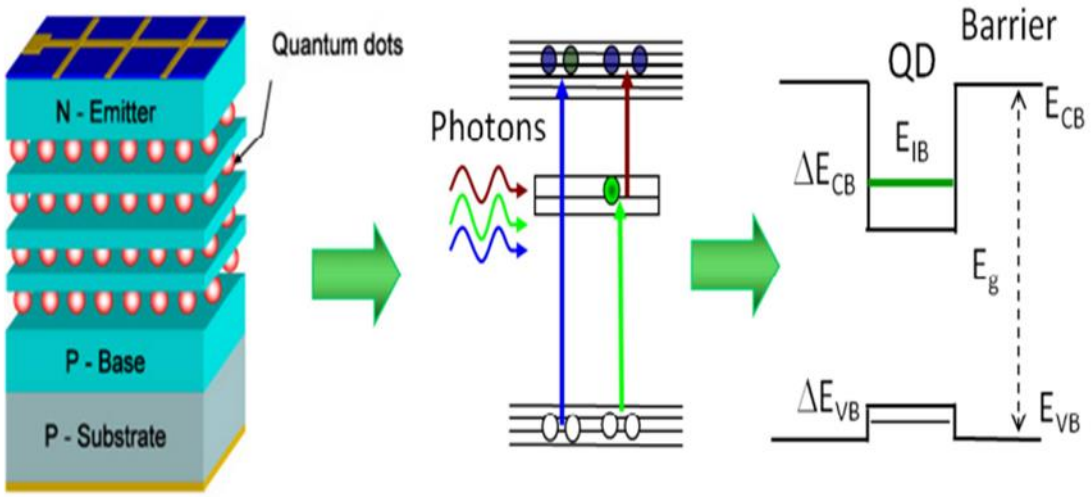

Figure 1.18: quantum dots solar cell.

I.8.3.4 Perovskite solar cells

perovskite solar cell is named after the material it is made of (perovskites). The perovskites are a group of compounds characterized by the general formula ABX3, which have the crystalline structure shown in figure 1.19 which displays a schematic figure of the generic ABX3 perovskite crystal structure for a hybrid organic–inorganic metal halide perovskite. The X position contains a halide anion, B is a metal cation, and A is an organic cation.[39] Current issues with perovskite solar cells revolve around stability (the material degrades in standard environmental conditions), thus drops in efficiency Broadly speaking [32].

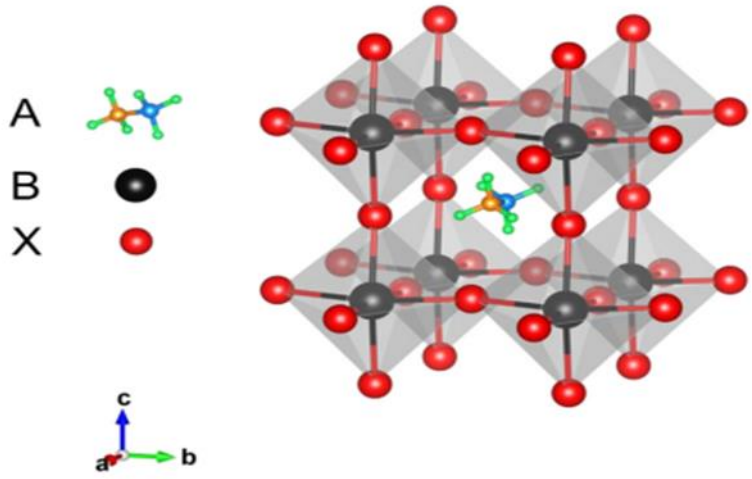

Figure 1.19: Crystal structure perovskite (CaTiO3) [39].

I.8.4 Fourth generation

the fourth-generation solar cells (the new generation) also known as inorganics in organics like hybrid perovskite.[31] it combines the low cost/flexibility of polymer thin films and the stability of novel inorganic nanostructures, the aim is to improve the optoelectronic properties of the low-cost thin-film PVs, as shown in figure 1.20. the architectures of This device are meant to maintain the inexpensive nature of PV device structure, but with the addition of inorganic components to improve the energy-harvesting cross-section Charge dissociation and charge transport in PV cells [5].

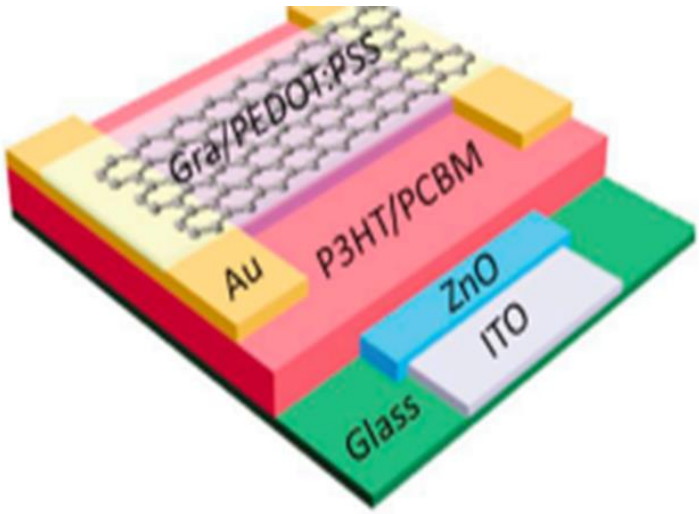

Figure 1.20: schematic representation and band structure of a PSC with the structure glass/indium tin oxide (ITO)/ZnO/P3HT:PCBM/Au/PEDOT:PSS/G [40].

From the above, we find that the difference in the four generations of cells is the difference in the material they are made of. These results of different values in solar cell characteristics, table 1.1 shows some values in different solar cells

Table 1.1: Confirmed single-junction terrestrial cell and submodule efficiencies measured under the global AM1.5 spectrum (1000 W/m2) at 25C°[27].

Classification	**Efficiency (%)**	**Area (cm^2)**	**V_{OC}(V)**	**J_{SC} (mA/ cm^2)**	**Fill factor (%)**	**Test centre (date)**	**Description**
Silicon							
Si (crystalline cell)	26.7 ± 0.5	79.0 (da)	0.738	42.65	84.9	AIST (3/17)	Kaneka, n-type rear IBC
Si (DS wafer cell)	24.4 ± 0.3	267.5 (t)	0.7132	41.47	82.5	ISFH (8/20)	Jinko Solar, n-type
Si (thin transfer submodule)	21.2 ± 0.4	239.7 (ap)	0.687c	38.50	80.3	NREL (4/14)	Solexel (35 μm thick)
Si (thin-film minimodule)	10.5 ± 0.3	94.0 (ap)	0.492c	29.7	72.1	FhG-ISE (8/07)	CSG Solar (<2 μm on glass)
III–V cells							
GaAs (thin-film cell)	29.1 ± 0.6	0.998 (ap)	1.127 2	29.78	86.7	FhG-ISE (10/18)	Alta Devices
GaAs (multicrystalline)	18.4 ± 0.5	4.011 (t)	0.994	23.2	79.7	NREL (11/95)	RTI, Ge substrate
InP (crystalline cell)	24.2 ± 0.5	1.008 (ap)	0.939	31.15	82.6	NREL (3/13)	NREL
Thin-film chalcogenide							
CIGS (cell) (Cd-free)	23.35 ± 0.5	1.043 (da)	0.734	39.58	80.4	AIST (11/18)	Solar Frontier
CdTe (cell)	21.0 ± 0.4	1.0623 (ap)	0.8759	30.25	79.4	Newport (8/14)	First Solar, on glass
CZTSSe (cell)	11.3 ± 0.3	1.1761 (da)	0.5333	33.57	63.0	Newport (10/18)	DGIST, Korea
CZTS (cell)	10.0 ± 0.2	1.113 (da)	0.7083	21.77	65.1	NREL (3/17)	UNSW
Amorphous/ microcrystalline							
Si (amorphous cell)	10.2 ± 0.3	1.001 (da)	0.896	16.36	69.8	AIST (7/14)	AIST
Si (microcrystalline cell)	11.9 ± 0.3	1.044 (da)	0.550	29.72	75.0	AIST (2/17)	AIST
Perovskite							
Perovskite (cell)	21.6 ± 0.6	1.0235 (da)	1.193	21.64	83.6	CSIRO (6/19)	ANU
Perovskite (minimodule)	18.6 ± 0.2	29.539 (da)	1.089	22.64	75.4	NREL (6/20)	UNCarolina, eight cells
Dye sensitized							
Dye (cell)	11.9 ± 0.4	1.005	0.744	22.47	71.2	AIST	Sharp

		(da)				(9/12)	
Dye (minimodule)	10.7 ± 0.4	26.55 (da)	0.754	20.19	69.9	AIST (2/15)	Sharp, seven serial cells
Dye (submodule)	8.8 ± 0.3	398.8 (da)	0.697	18.42	68.7	AIST (9/12)	Sharp, 26 serial cells
Organic							
Organic (cell)	15.2 ± 0.2	1.015 (da)	0.8467	24.24	74.3	FhG-ISE (10/20)	Fraunhofer
Organic (minimodule)	12.6 ± 0.2	26.129 (da)	0.8315	21.32	71.1	FhG-ISE (9/19)	ZAE Bayern (12 cells)
Organic (submodule)	11.7 ± 0.2	203.98 (da)	0.8177	20.68	69.3	FhG-ISE (10/19)	ZAE Bayern (33 cells)

All the development and improvements of all types of solar cells according to efficiency value over the years can be summarized, as shown in the figure 1.21

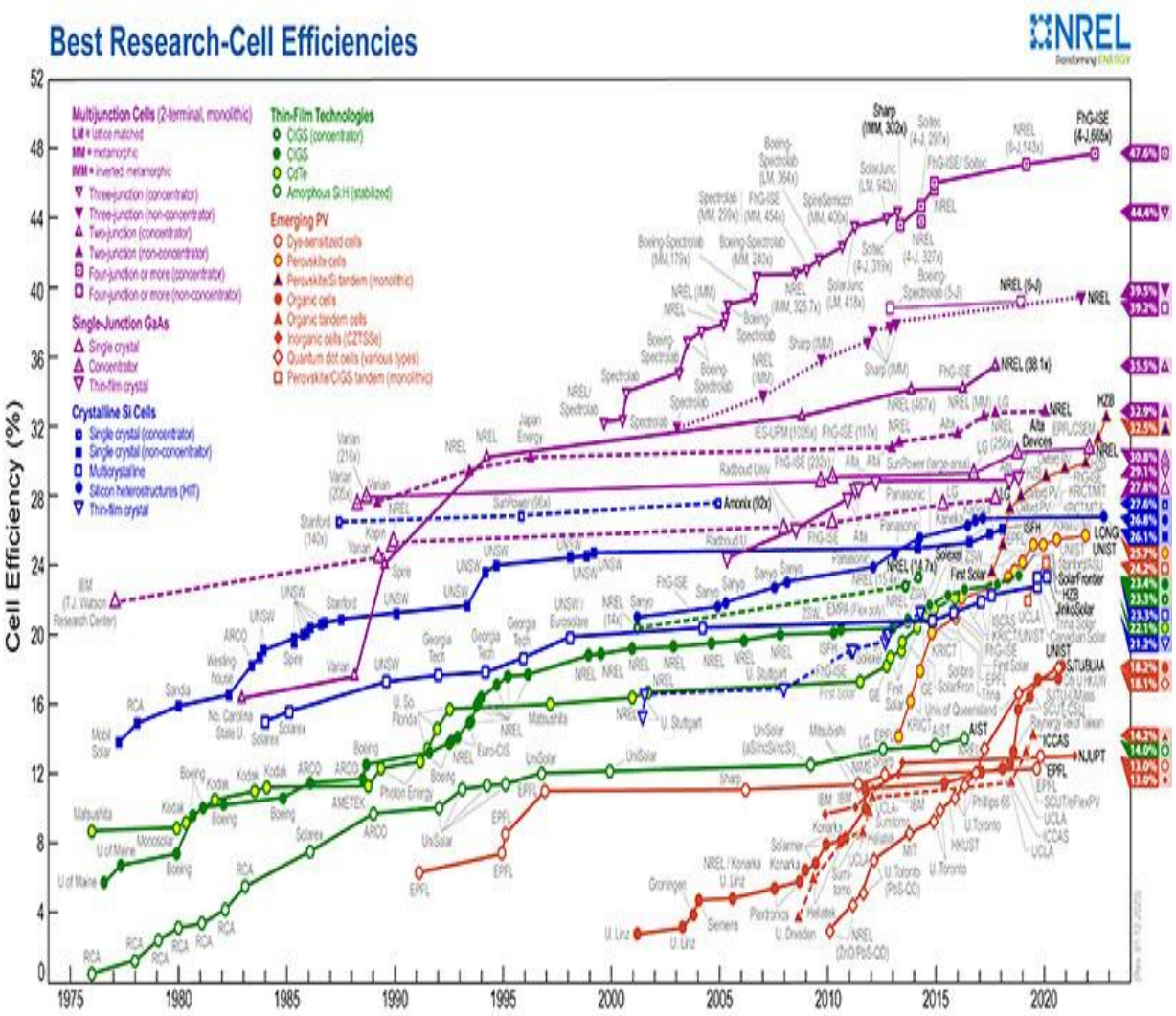

Figure 1.21: best research-cell Efficiencies [41].

Chapter II

II.1 Introduction

The semiconductor material has experienced development from appearing to now. It can be as the building blocks of all modern technologies, where, they form the basis of all diodes, transistors, integrated circuits, and microprocessors.

This chapter focuses on some semiconductor materials (graphene, silicon, GaAs, InP) and their properties.

II-2 Graphene

In 2010. The Nobel Prize in Physics is awarded to Andre Geim and Konstantin Novoselov for their breakthrough discovery in 2004, which Represented the successful isolation of a graphene that is extracted from graphite. Graphene is a two-dimensional (2D) material, it is a single-layer hexagonal lattice of carbon atoms that forms the honeycomb crystal structure, as shown in figure 2.1. Graphene is formed from a unit cell, with a lattice constant of $a = 0.246$ nm, and is formed of two independent carbon sites, where the strong σ-bonds and weak π bonds of the carbon atoms give a bond length of 0.142 nm. it is considered as well as a promising candidate material for future applications in carbon-based nanoelectronics and molecular devices [42].

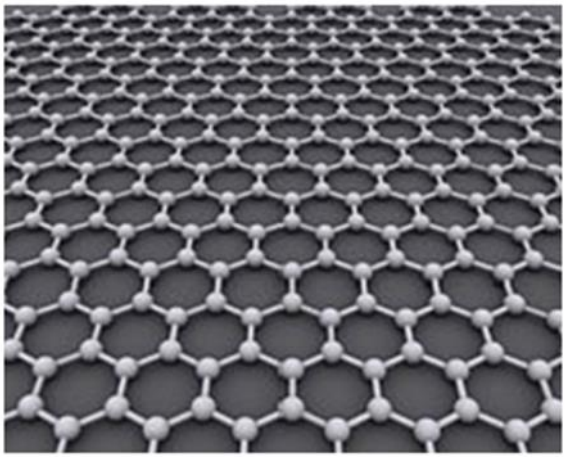

Figure 2.1: The structures of graphene [43].

II.3 Synthesis of graphene

Graphene has several methods of synthesis, which can be divide into two: bottom-up and top-down, as shown in figure 2.2 [44].

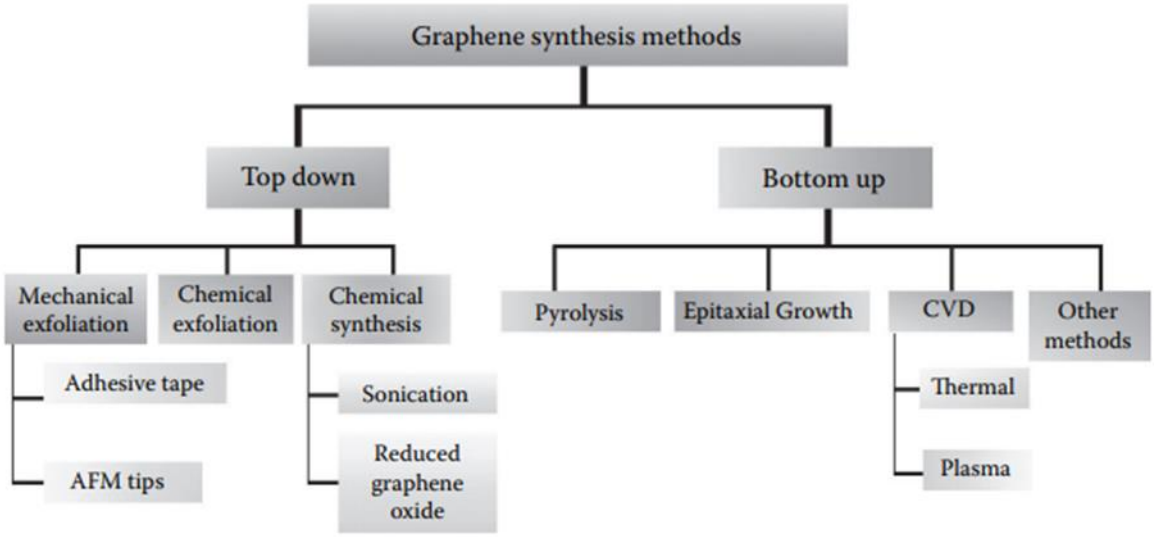

Figure 2.2: the schematic represents the different graphene synthesis methods [44].

From all the methods of synthesis, catalytic thermal Chemical vapor deposition (CVD) has been proved to be one of the best processes for large-scale graphene fabrication [44]. CVD is a simple, scalable, and cost-efficient method to prepare single and few-layer graphene films on various substrates it opens a new route to large-area production of high-quality graphene films for practical applications. Figure 2.3 shows typical chemical vapor deposition system for graphene synthesis [45].

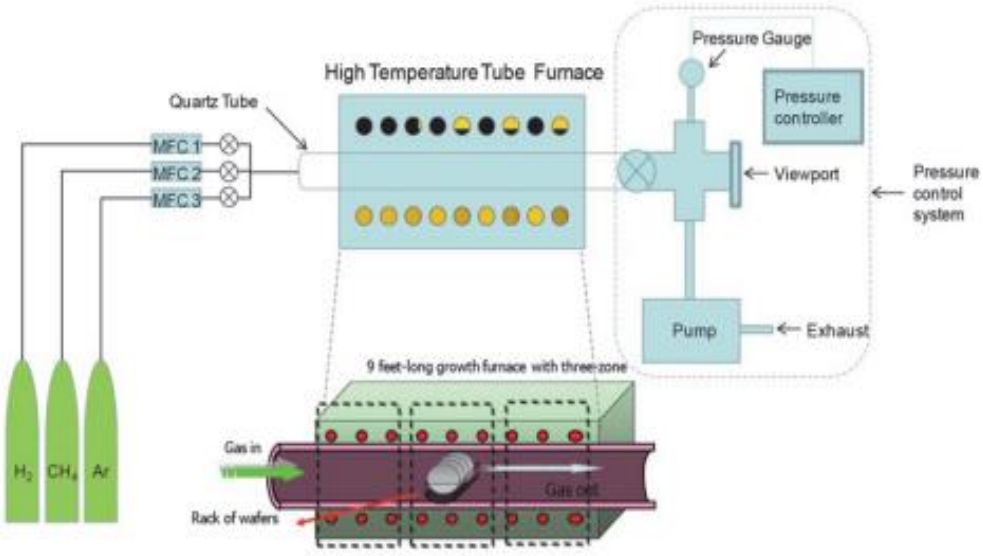

Figure 2.3: complete apparatus setup for chemical vapor deposition of graphene [45].

Thermal chemical vapor deposition (CVD) is a chemical process It happened at high temperatures by which a substrate is exposed to thermally decomposed precursors and the desired product is deposited onto the substrate surface. Because the high temperature is not desired in many cases, plasma-assisted decomposition and reaction may lower the process temperature. Figures 2.4 (a) and 2.4 (b) demonstrate the schematic of thermal and plasma-enhanced CVDs (PECVD). Example formation of single- to few-layer of CVD graphene over the Ni surface as shown in HRTEM in Figures 2.5 [44].

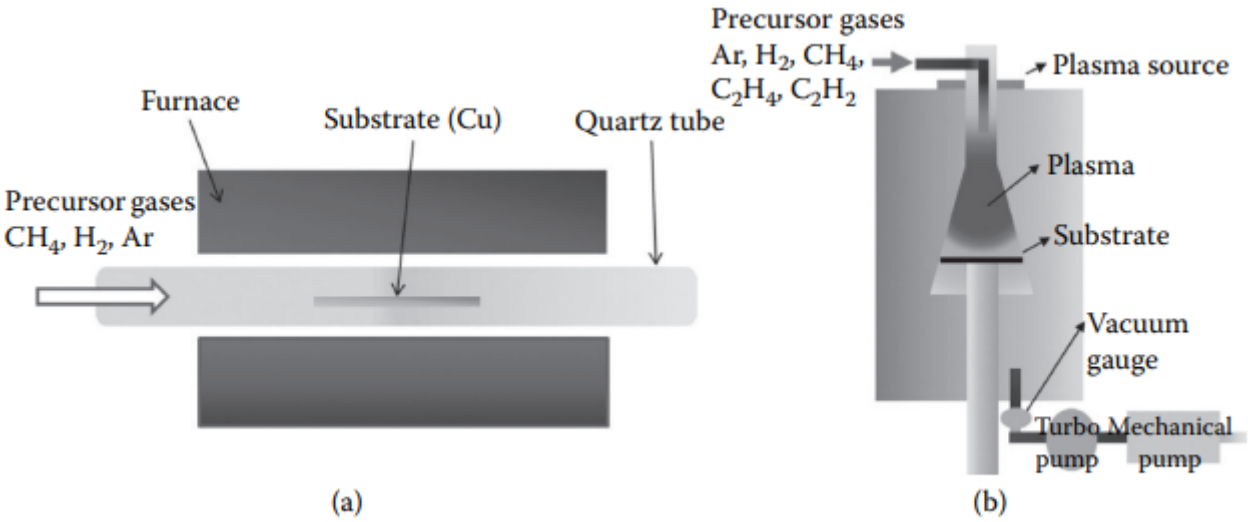

Figure 2.4: schematic of (a) thermal CVD and (b) plasma-enhanced CVD (PECVD) [44].

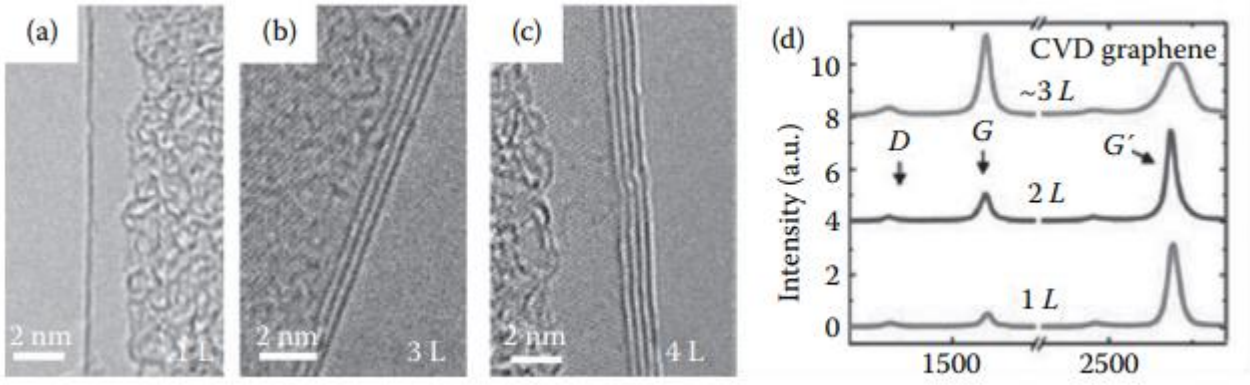

Figure 2.5: (a), (b) and (c) HRTEM images confirming the formation of thermal CVD grown mono- to few-layer graphene on Ni and (d) representative Raman plot for successive layers of graphene. by chemical vapor deposition [44].

Where (HRTEM) is high-resolution transmission electron microscopy.

The next table 2.1, concentrate on the properties of obtained graphene with some advantages of synthesis methods.

Table 2.1: various methods of synthesizing graphene [43].

Method of synthesis	**Properties of obtained graphene and advantages of the method**
CVD method	• One-layer graphene is obtained using copper as a catalyst. • Graphene with high quality. • Inexpensive and realistic method to obtain multilayered graphene. • Ability to scale up production
Wet-chemistry approach	• Compared to exfoliation and epitaxial growth, it is more versatile. • Ease of scaling up. • Alteration of the electronic, optical, and mechanical properties of graphene may occur as obtained graphene is partially synthesized.
Exfoliation and cleavage method	• Graphene possesses excellent electrical and structural quality. • It is the simplest method, although it leads to the formation of uneven graphene films. • The simplest and earliest method.
Epitaxial growth method	• Graphene with multilayered structure is obtained. • Ability to control the number of layers formed is made possible. • Graphene obtained via this route has limited application in biomedicine. • Graphene synthesized through this method is difficult to functionalize. • It is difficult to functionalize graphene obtained via this route.

II.4 Graphene properties

In recent years, graphene created enormous research activities due to its excellent optical, electrical, and mechanical properties, most of the applications are still in their infancy [44]. We will learn now about the most important physical properties: mechanical, Thermal, Electronic, Optical properties, and other properties:

II.4.1 Mechanical properties

The strongest material ever is the first title for graphene received after the confirmation of sustaining breaking strengths of 42 N/m with an intrinsic mechanical strain of ~ 25% and of young modulus of Y ~ 1.0 TPa, which can also control Its thickness mechanical. The outstanding mechanical properties of graphene have also attracted interest from electronic applications due to the potential use that these light, stiff, and flexible materials can offer for designing building-block components in nanoelectromechanical systems (NEMS). which requires a complete correspondence between mechanical and electrical responses of the conductive channel. The operation mechanism relies strictly on the feasibility of band gap engineering with the aid of external mechanical forces [44].

II.4.2 Thermal properties

Graphene has an extraordinarily high room temperature (RT) carrier mobility exceeding $15{,}000\ cm^2V^{-1}s^{-1}$ and the electric field effect is tunable with either electrons or holes as charger carriers with a concentration of $\sim 10^{13}\ cm^{-2}$. In addition, conductance quantization possibilities of inducing a band gap through lateral quantum confinement effects and prospects of epitaxial growth make graphene a promising material for future electronic circuits. There have been theoretical suggestions that graphene has an unusually high thermal conductivity. But there was no experimental measurement reported to support the claim of these theoretical works before 2008. the initial experimental and theoretical studies of thermal conduction stimulated several other research studies in this field, which results from thermal conductivity values as shown in figure 2.6, compared to previously reported values [44].

The research group that repeated the measurements using the micro-Raman spectroscopy-based technique found the value of thermal conductivity is $630\ W/mK$ for suspended graphene at $T \approx 600$ K. The graphene membrane was heated to $T = 660$ K in the center and above~500 K over most of its area because the measurements were conducted at ambient [44].

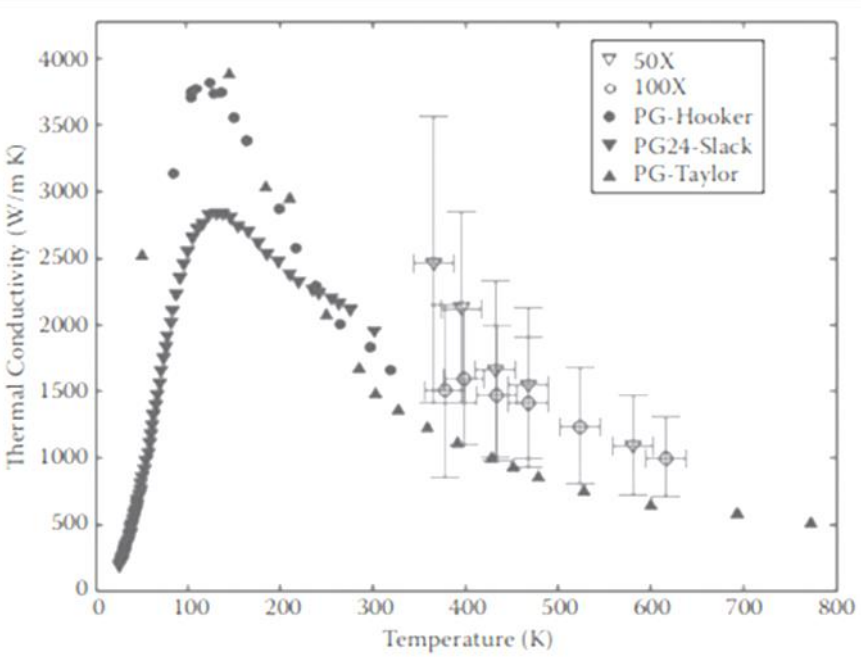

Figure 2.6: The thermal conductivity of the suspended CVD graphene was measured using the 100X and 50X objective lens as a function of the measured graphene temperature [44].

II.4.3 Electronic properties

Graphene is a gapless semiconductor with unique electronic properties resulting from the fact that charge carriers in graphene obey linear dispersion relation, which leads to the observation of many interesting electronic properties: electron mobility is extremely high, with reported values exceeding 15,000 $cm2/Vs$ at room temperature, low resistivity, improved current capacity, and temperature conditions, also graphene is thought to operate at terahertz frequencies or trillions of operations per second [46, 47].

II.4.4 Optical properties

Like other properties, graphene has many interesting optical Properties which is:

- It has an exceptionally high absorbing capacity (for an atomic monolayer) of white light $\pi\alpha = 2.3\%$, where α is the fine structure.
- Graphene can be easily saturated in the visible to near-infrared range under strong excitation because of its universal optical absorption [47].

II.4.5 other properties

Graphene is considered an impermeable material. where a single layer of atoms can act as a perfect barrier to liquids and gases. However, graphene pores (defects) can selectively permit the passage of water and gas molecules, letting graphene be tuned to allow selective gas permeability [47].

II-5 Graphene application

Due to different properties, graphene has several applications as shown in table 2.2.

Table 2.2: different graphene applications [47]

usage	**Applications**
Membranes	• Using electricity to control the flow of water through graphene membranes. • Gas barriers, such as those found in food packaging. • Demineralization and purification of water. • Organic solvent separation from water.
Electronics	• Devices that are stretchable, flexible, and foldable. • Printable electronics at a low cost. • Electronic equipment with high frequencies. • Transistors with superior efficiency. • Nano-electronics thermal management and heat dissipation. • Because graphene's optical properties can be governed through doping, it's quite well for optoelectronic devices (electrical devices that source, detect, and control light)
Biomedical technologies	• Thermal ablation of cancer cells with high resistance. • Detection and neutralization of cancer stem cells. • Bioelectronics (bionics). • Electronics can contact with living cells and nerve tissue. • Bioimaging with luminescent graphene tags.
Sensors	• Detection of explosives. • Biosensor for detecting Parkinson's disease biomarkers and bacteria. • Specific gas detection. • Tattoos with self-healing, multifunctional electronic sensors. • Observing the environment.
Energy	• Graphene increases the energy capacity as well as the charge rate of

harvesting and storage	rechargeable batteries. • Activated graphene essentially produces superior supercapacitors, which are required for energy storage. • Graphene electrodes could pave the way for a promising approach to producing solar cells that are low-cost, flexible, and lightweight. • Experimentation designs for graphene-based solar cells in which graphene serves as various components of the cell. • Multifunctional graphene mats are promising catalytic system substrates. • Proton transport in graphene holds promise for mimicking photosynthesis artificially
Composites and coatings	• Body structures made of lightweight composites. • Lubricants with improved anti-wear characteristics. • Nano-laminates as high-permeation barrier films. • Corrosion resistance. • Translucent conductive coating for solar devices. • Protection from lightning strikes and radiation shielding. • Coatings that are superhydrophobic. • Thin films that are translucent, conductive, and flexible. • Highly effective electromagnetic interference (EMI) shielding sheets.

with all graphene applications in different areas, in this work, we focus on user of graphene solar cells, in which graphene serves as various components of the cell where it was used as the electrodes (transparent anodes, non-transparent anodes, transparent cathodes, and catalytic counter electrodes), or as the active layer (light-harvesting material, Schottky junction, the electron transport layer, hole transport layer, both hole and electron transport layer, and interfacial layer in the tandem configuration) [48].

II.6 Silicon

Next to oxygen, silicon is a unique material, it is the second most abundant element in the Earth's crust. exists mainly in the oxidized silicate (SiO2) form. So, silicon abundance is one of the reasons it is used for a wide range of purposes like the electronics industry which crystalline silicon is the most widely used semiconductor in it. The most common commercial applications are photovoltaics Which considers 90% of terrestrial solar cells made from

silicon, with a lifetime of up to 30 years. So, it can be said that silicon is the heart of both modern and future technology [49].

II.6.1 define silicon material

Silicon (Si) is a semiconductor material from group IV of the periodic table of the elements, as shown in figure 2.7. Silicon crystallizes into a diamond cubic crystal structure, which is two fcc structures shifted along the diagonal with respect to each other, as shown in figure 2.8. The chemical bond is purely covalent [50-52] [51]. silicon is limited in its use in optoelectronic applications where semiconductors such as GaAs and InP dominate this field that is because silicon has an indirect band gap of 1.12 eV and emits light weakly near the infrared region by phonon assistance [49].

Figure 2.7: periodic table partial [53].

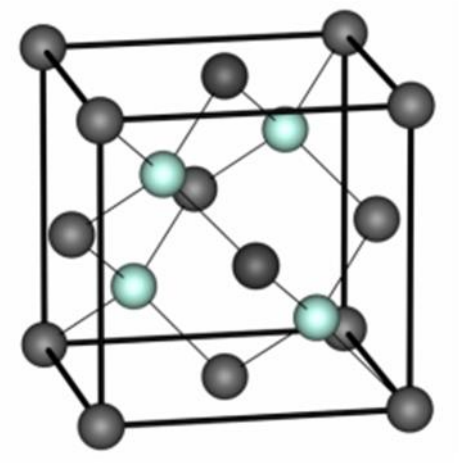

Figure 2.8: Silicon crystallographic structure [52].

II.6.2 Silicon properties

Table 2.3 summarizes the important properties of silicon.

Tible2.3: silicon properties [50]

Parameters	**Silicon**
Atomic number of Si	14
Atomic mass of Si	28 (92.23%)
Crystal structure	diamond
Lattice constant (nm)	0.5431
Si atoms (atoms.cm^{-3})	$5 * 10^{22}$
Melting point (K)	1687
Specific density (g.cm^{-3} at 298 K)	2.329
Specific density (liquid) (g.cm^{-3})	2.57
Thermal conductivity ($W.m^{-1}$)	149
Coefficient of thermal expansion [$m^{-1}K^{-1}$ (at 298K)]	$2.56 * 10^{-6}$
Specific heat capacity	19.79 ($J.mol^{-1}K^{-1}$) 0.705($J.g^{-1}K^{-1}$)
Young's modulus (GPa)	150
Speed of sound ($m.s^{-1}$)	8433
Hardness (Mohs)	7

Hardness [$kg.mm^{-2}$ (Knoop hardness)]	850
Volumetric compression coefficient (kPa^{-1})	$1.02 * 10^{-8}$
Index of refraction (varies with temperature and λ)	~3.54 (λ 1.1 μ m, RT) ~3.48 (λ 2 μ m, RT)

Where RT is room temperature.

II.6.3 Silicon/graphene Schottky solar cells

Because of the unique structure and fascinating properties of graphene, this material has received a lot of research attention especially for use to develop electronic devices. where considered the graphene-Schottky junction solar cells are more attractive for study. In 2010 Manufactured graphene/silicon Schottky junction solar cell that a layer of SiO2 is applied onto an n-Si substrate and etching the layer exposes a square window which defines the active area of the solar cell with predeposited Au line contacts around after that a film consisting of thin-layer graphene was coated conformally. Was selected n-type from silicon to create a Schottky barrier by knowing the value of the work function of graphene and silicon, as shown in figure 2.9 [54].

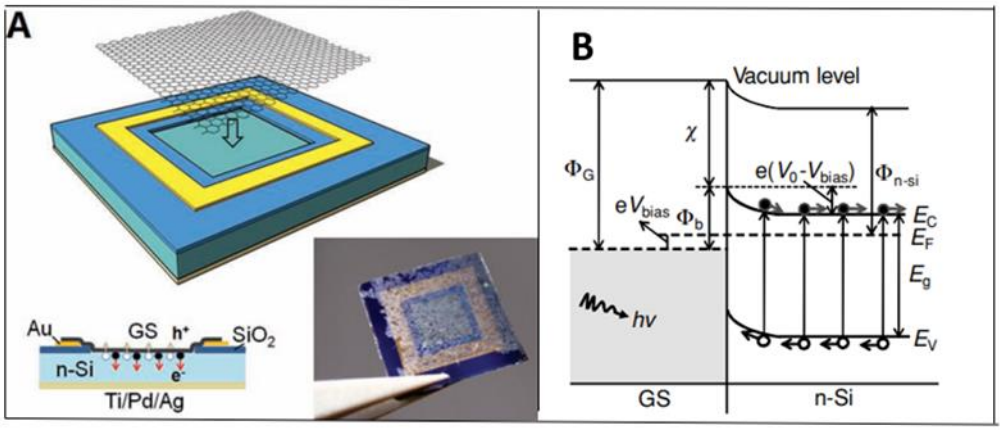

Figure 2.9: A) schematic illustration, and photograph to GS/n-Si Schottky cell with a 0.1 cm^2 junction area. B) Energy diagram of the forward-biased GS/n-Si Schottky junction upon illumination [54].

Although graphene on silicon solar cells attracted significant attention, its power conversion efficiency is generally smaller than 4% without chemical doping treatments, it is mainly limited by the low work function of Gr and high-density defect states at the Gr–Si interface. So, in 2014 reported a new structure of Gr–Si solar cells by introducing a graphene oxide (GO) interlayer to engineer the Gr–Si interface for improving device performance. As shown in figure 2.10. The Gr/GO/Si solar cells can be achieved 6.18% as maximum efficiency and are more stable than the Gr–Si solar cell with chemical doping [55].

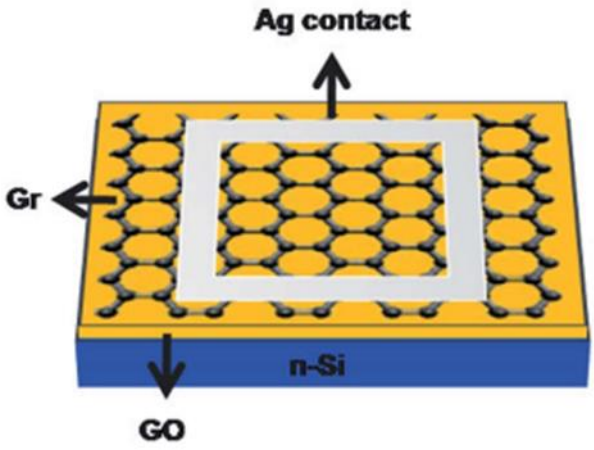

Figure 2.10: schematic illustration of a Gr/GO/Si solar cell [55].

II.7 GaAs

II.7.1 define GaAs material

GaAs is a III–V compound semiconductor composed of the element gallium (Ga) from column III (which is a rare element produced as a by-product in Al or Zn production) and the element arsenic (As) from column V (which is mainly produced from sulfur ores such as As_2S_4 or As_2S_3) of the periodic table of the elements. It is consisting of two F.C.C. lattices overlapping with each other and from the other one is shifted by a quarter [56, 57], as shown in the figure 2.11.

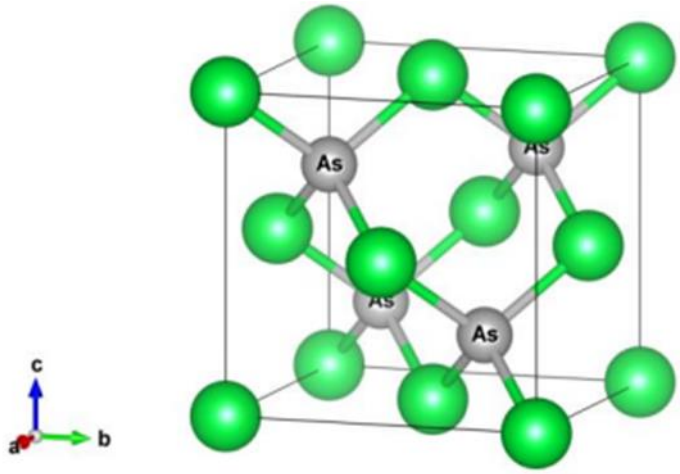

Figure 2.11: Zinc blende crystal structure of GaAs [58].

II.7.2 GaAs properties

The next table 2.4 summarizes the important properties of GaAs.

Table 2.4: GaAs properties [59].

Parameters	**GaAs**
Band gapE_g(eV)	1.42
Electron affinity $\chi(eV)$	4.07
Dielectric constant ε	12.9
Effective conduction band density$N_C(10^{17}cm^{-3})$	4.7
Effective valence band density $N_V(10^{18}cm^{-3})$	9
Electron mobility $(cm^2/V.s)$	4000
Hole mobility(cm^2/Vs)	200

II.7.3 GaAs/graphene Schottky solar cells

Due to the direct bandgap of GaAs and its highly resistant to radiation, in comparison with currently widely used Si. it makes GaAs solar cells take over from silicon as the conventional cell type desirable for space applications. For this, the graphene on GaAs Schottky solar cells have got research attention too, to form Schottky junctions Chemical-vapor-deposited graphene sheets have been transferred onto n-type GaAs substrates. Before transferring graphene, SiO2 layer was deposited on the substrate, which act as an insulating

layer to prevent the formation of contact between the top electrode and the semiconductor (GaAs) considering the discontinuity of large-area graphene prepared by CVD. As shown in figure 2.12 [60].

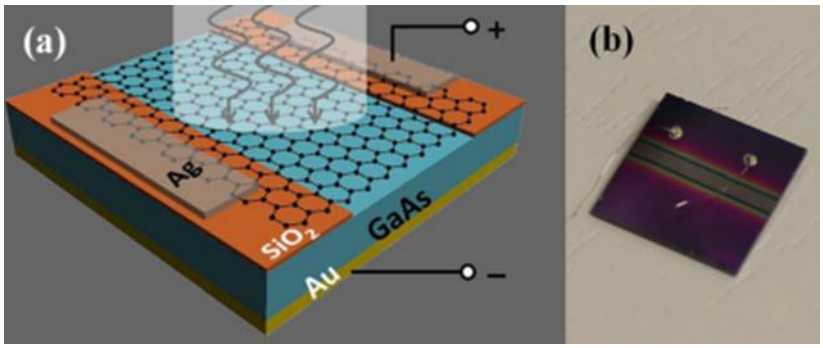

Figure 2.12: (a) the schematic of Ag/graphene/GaAs/Au hybrid system with SiO2 as an insulating layer. (b) Photograph of the graphene/GaAs junction solar cell [60].

II.8 InP

InP as a compound semiconductor material is very promising to use in many applications such as high-frequency devices, millimeter wave communications, anticollision systems, imaging sensors, optoelectronic integrated circuits (OEICs) with the integration of lasers, photodetectors and amplifiers are indispensable for the second-generation communication systems with 40 Gb/sec. Some of the compound semiconductors have band gaps of around 1.4 eV are promising for solar cells because they assure high energy conversion efficiencies. InP, one of these compound semiconductors, it is also promising as solar cells for space satellites because of its high resistivity against radiation.

II.8.1 define InP material

InP is a compound semiconductor between indium which is recovered as a Raw by-product from zinc and lead smelting and purified from impurities by a process such as the zone-melting method, and phosphorus which is recovered from fluorine apatite $(Ca_5(PO_4)_3F)$ to produce yellow phosphorus that is flammable, red phosphorus which is more stable at room temperature and produced from yellow phosphorus by a thermal conversion process. InP has a zinc blend structure as other III-V materials as seen in figure 2.13. Indium and phosphorus atoms form a face-centered cubic structure respectively, these structures are superimposed with a deviation to the position (1/4, 1/4, 1/4). Indium atoms are

therefore surrounded by four phosphorus atoms and phosphorus atoms are also surrounded by four indium atoms so that they make tetrahedral bindings [61].

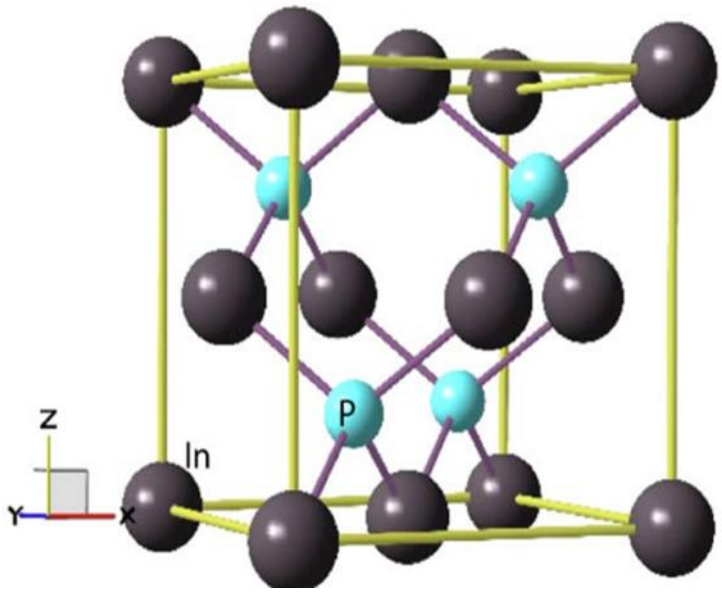

Figure 2.13: unit cell structure of InP [62].

II.8.2 InP properties

The next table 2.5 summarizes the important properties of InP.

Table2.5: InP properties [61].

Crystal structure	**Zinc blend**
Lattice constant	5.869 A
Density	4.787 g/cm^3
Melting point	1335 K
Vapor pressure at melting point	27.5 atm
Linear expansion coefficient	4.5 $\times$ 10^{-6} /deg
Thermal conductivity	0.70 W/cm. K
Dielectric constant	12.5
Band gap at room temperature (RT)	1.35 eV
Optical transition type	Direct
Intrinsic carrier concentration at RT	2.0 $\times$ 10^7 cm^{-3}
Intrinsic resistivity	8.2 $\times 10^7$ $fi - cm$
Electron mobility at RT	4,500 cm²/V s

Hole mobility at RT.	150 $cm^2/V\ s$
Melting point	1070 (°C)
Stacking fault energy	20 (erg/cm^2)
Critical resolved shear stress	0.36 (MPa)

II.8.3 InP/graphene Schottky solar cells

InP solar cells exhibit features compared to other solar cells like higher resistance to space radiation damage compared to Si and GaAs solar cells, thus InP based solar cells may be promising for space applications. So, the graphene/InP Schottky junction could be a candidate for solar cells, these cells depend on the same previous structure which was used in graphene/GaAs Schottky solar cell, as shown in figure 2.14 [63].

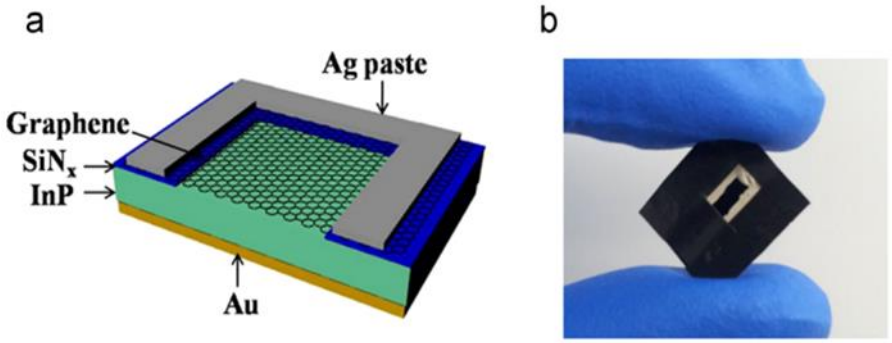

Figure 2.14: (a) schematic structure of graphene/p-InP Schottky junction device. (b) A digital photograph of finished graphene/p-InP solar cell [63].

Chapter III

III.1 Introduction

simulation is considered the best way to study any semiconductor device with saving time and money. In this work, we will simulate a graphene Schottky junction solar cell by using the simulation software SILVACO (TCAD).

III.2 Silvaco

Silvaco is a program that allows the creation, optimization, and characterization of semiconductor devices by simulation, Silvaco has many subunits which have different uses such as DeckBuild, TonyPlot, and ATLAS.

III.2.1 DeckBuild

DeckBuild is an interactive interface in Silvaco, it allows information input of the semiconductor device to simulate the process of manufacturing or working of the device and it is an extremely powerful and flexible tool that is easy to use for a transparent transition from one simulator to another. Figure 3.1 shows the interface of DeckBuild.

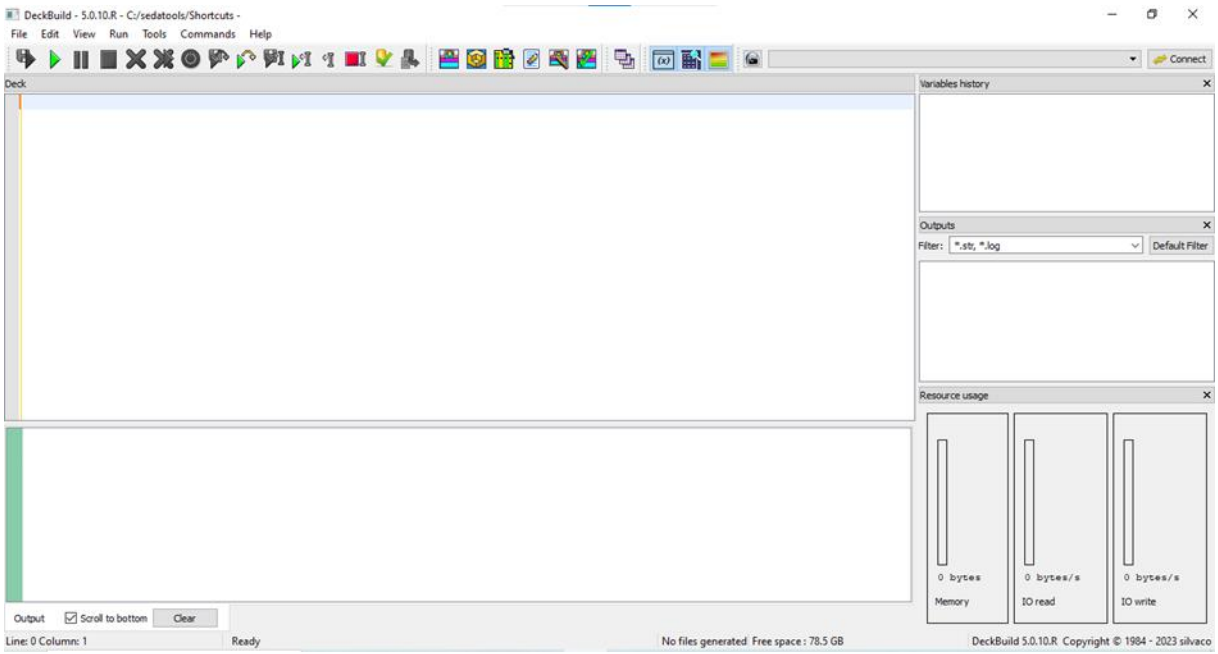

Figure 3.1: DeckBluid window.

III.2.2 TonyPlot

TonyPlot is an interactive tool that allows drawing the results obtained from the simulation. TonyPlot can operate stand-alone or along with other interactive tools, such as DeckBuild. TonyPlot graphs Scan be as a curve or Structure as shown in figure 3.2.

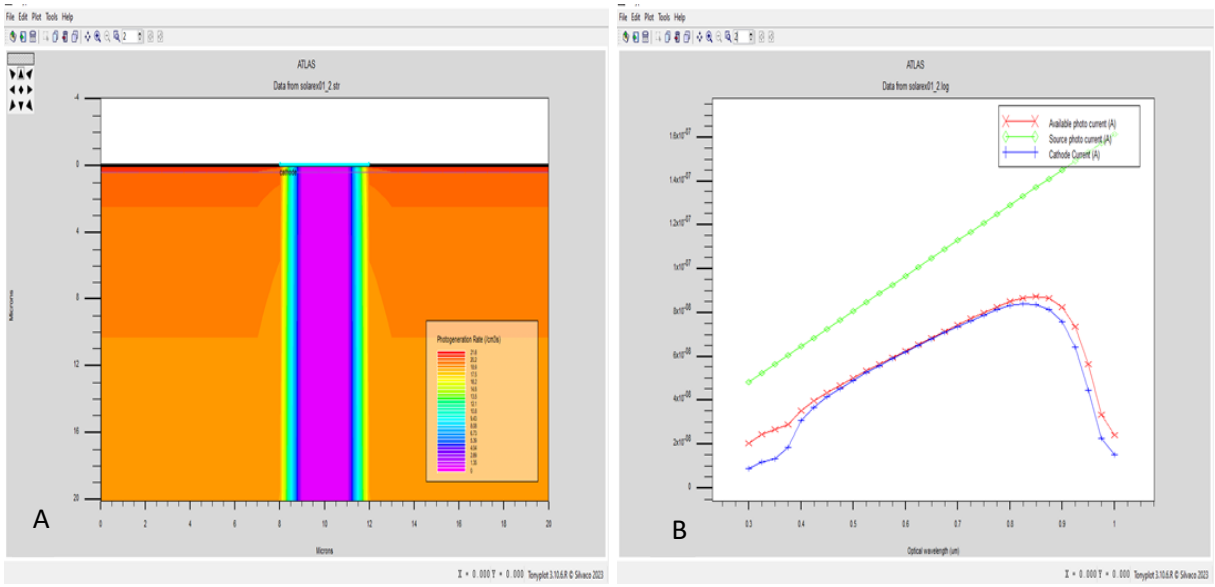

Figure 3.2: graphs illustrated using TonyPlot A) structure solar cells, B) spectral response curve.

III.2.3 Silvaco ATLAS simulation software

ATLAS software of Silvaco provides general capabilities for two and three-dimensional simulation of semiconductor devices thanks to an available comprehensive set of physical models. ATLAS works well with other software from Silvaco such as DeckBuild which represents an interactive run-time environment, and TonyPlot which draws the graphics and analysis.

III.2.4 Atlas inputs outputs

Most ATLAS simulations use two types of input files: the first is a structure file that defines the structure that will be simulated, and the second is a text file that contains commands for ATLAS to execute. ATLAS produces three output files: run-time output (gives you the progress and the error and warning messages as the simulation proceeds), log file (stores all terminal voltages and currents from the device analysis), and solution file (stores 2D and 3D data relating to the values of solution variables within the device). As shown figure 3.3.

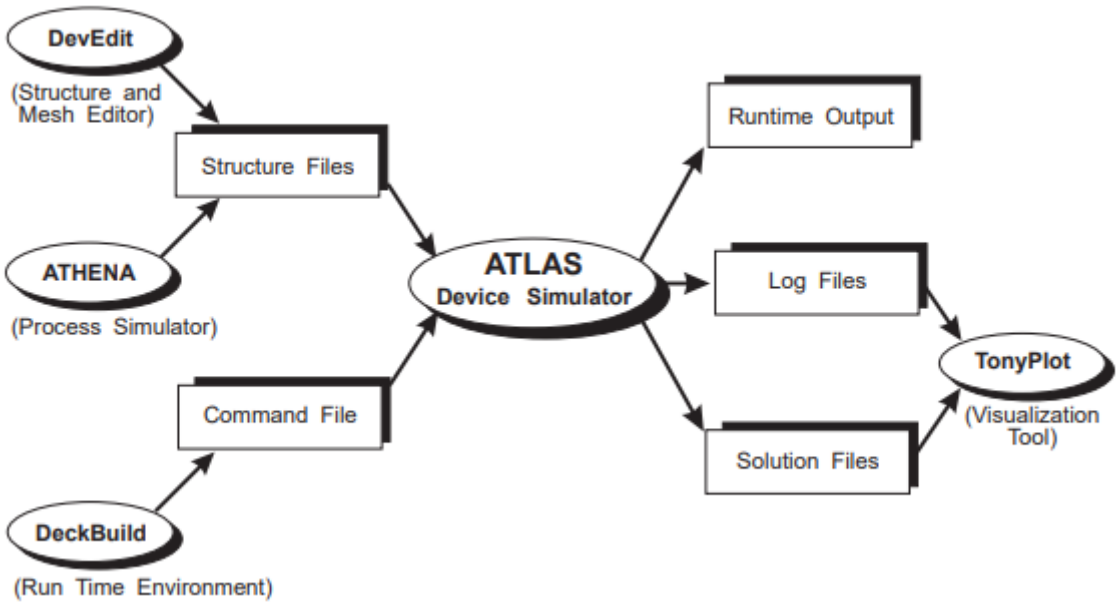

Figure 3.3: ATLAS inputs and outputs.

III.3 Atlas syntax

An ATLAS command file is a list of commands for ATLAS to execute. This list is saved as a text file that can be prepared in DeckBuild or using any text editor.

III.3.1 Statements and Parameters

The keyword and a set of parameters are the general formats of statements in the input file which contains a sequence of statements. Such as:

<STATEMENT> <PARAMETER> = <VALUE>

ATLAS may have four different types for the <VALUE> parameter to any <STATEMENT>, the <VALUE> can be: real, integer, character, and logical.

III.3.2 The order of atlas commands

The order of statements in the ATLAS input file is important. Failure to do the correct order may lead to error message that produces incorrect operation or termination of the program. In ATLAS statements there are five groups of statements that must occur in the correct order as shown in figure 3.4.

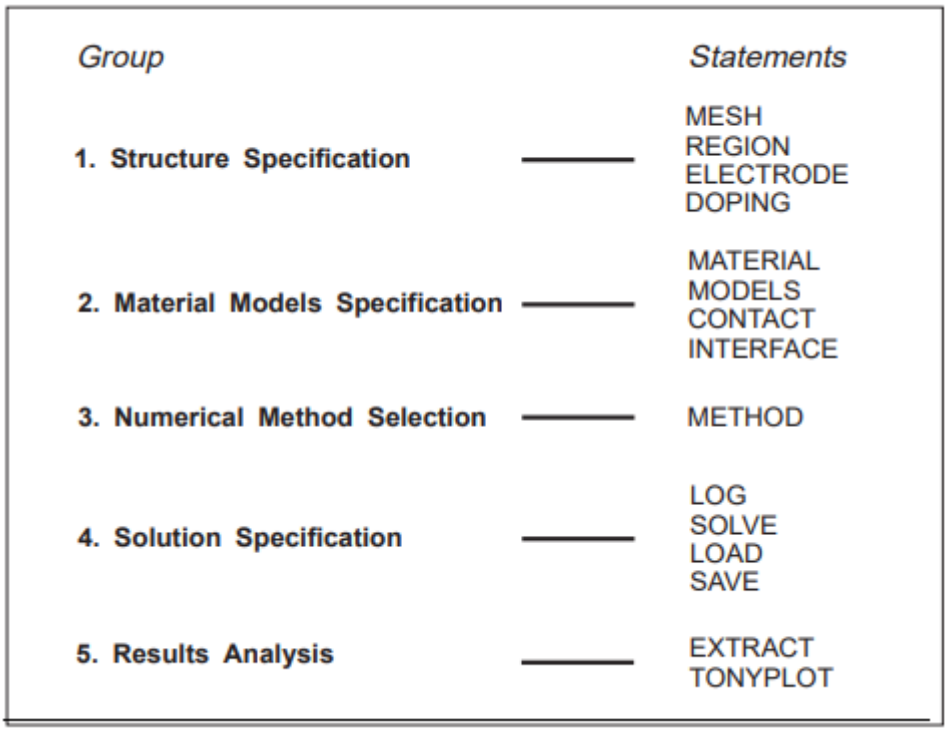

Figure 3.4: ATLAS command groups with the primary statements in each group.

III.4 Defining a structure

To defined a device structure in ATLAS, there are three different ways:

1. Read an existing structure from a file.
2. Transfer the input structure from ATHENA or DEVEDIT by using the automatic interface feature from DeckBuild.
3. Create a structure by using the ATLAS command language.

III.4.1 Specifying mesh

Mesh is the first statement in defining a structure because it covers the physical simulation domain, and it is a two-dimension grid that can control it. The next statement is used to define the mesh:

MESH SPACE.MULT=<VALUE>

X.MESH LOCATION=<VALUE> SPACING=<VALUE>

Y.MESH LOCATION=<VALUE> SPACING=<VALUE>

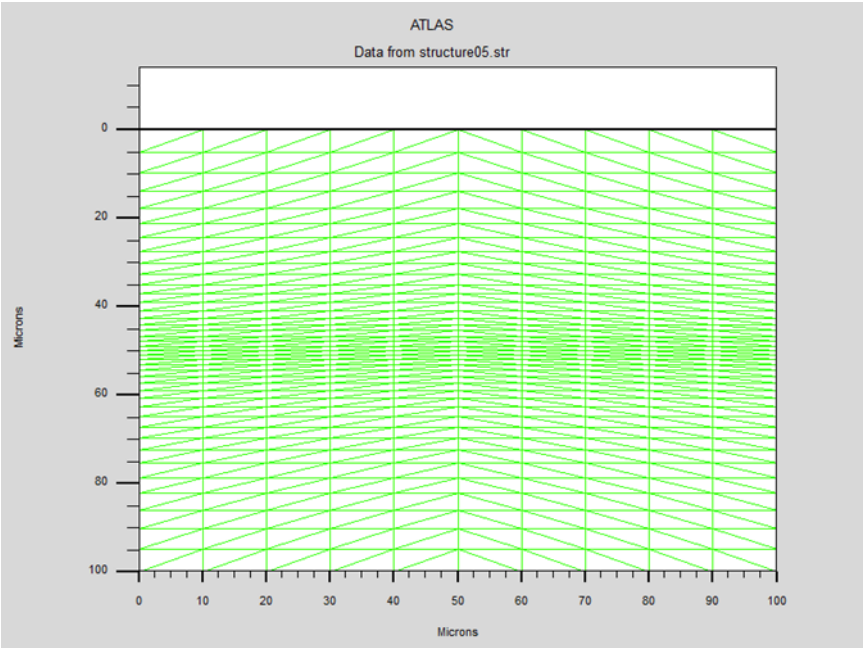

Figure 3.5: mesh created using ATLAS syntax.

III.4.2 Specifying regions and materials

After Specifying the mesh, every part of it must be assigned a material type. This is done with REGION statements, as shown in figure 3.6. ATLAS can have up to 200 different regions specified by following statement:

REGION number=<integer> <material_type> <position parameters>

Number of regions must start at 1 with increased for each subsequent region statement.

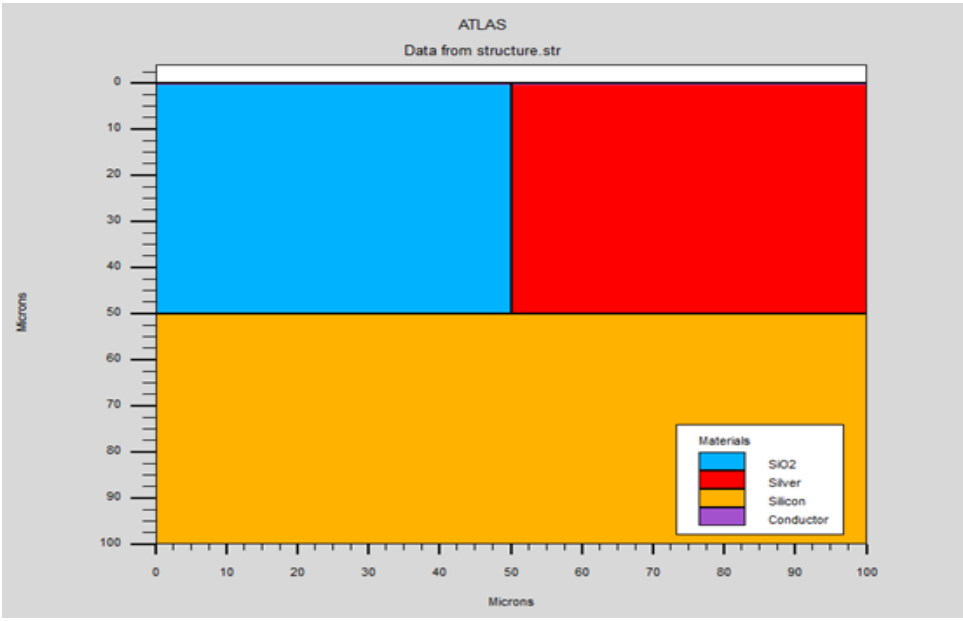

Figure 3.6: Atlas regions with materials defined.

III.4.3 Specifying electrodes

When specifying structure, at least one electrode that contacts a semiconductor must be defined. This can be done using the electrode statement as follows.

ELECTRODE NAME=<electrode name> <position_parameters>

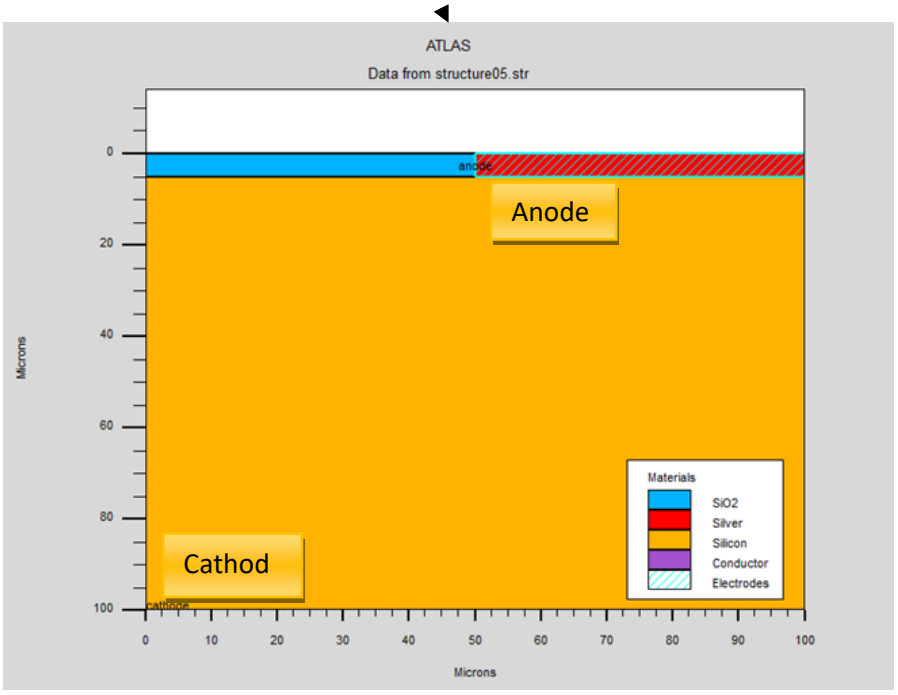

Figure 3.7: Atlas electrodes.

III.4.4 Specifying doping

DOPING statement is another ATLAS statement, which is used to specify the doping. For example:

DOPING <distribution_type> <dopant_type> <position_parameters>

The parameters of the DOPING statement differ by doping distribution, for example:

- DOPING UNIFORM CONCENTRATION=1E16 N.TYPE REGION=1
- DOPING GAUSSIAN CONCENTRATION=1E18 CHARACTERISTIC=0.05 P.TYPE X.LEFT=0.0 X.RIGHT=1.0 PEAK=0.1

III.5 Defining material parameters and models

III.5.1 Specifying contact characteristics

An electrode in contact with semiconductor material is assumed by default to be ohmic if not defined by his work function. The Contact statement is used to specify the metal

work function where the Name parameter is used to identify which electrode will have its properties modified. For example:

CONTACT NAME=anode WORKFUNCTION=4.9

III.5.2 Specifying material properties

In ATLAS, there is a rich collection of materials that have been defined but this does not preclude the definition of a new material. Which can be using MATERIAL statement as follows:

<Material> <Material> = <VALUE>

Due to the split of materials (semiconductors, insulators, and conductors). Each class requires a different set of parameters to be specified. For example, the following statement is for defining graphene as a semiconductor:

Material material=graphene EG300=0.026 MUN=16983.69 MUP=16983.69 NC300=2e16 NV300=2e16 affinity=5 PERMITTIVITY=6 index.file=graphene.nk user.group=semiconductor user.default=4H-SIC out.index=graphene

III.5.3 Specifying physical models

To get accurate results, simulation should be to a realistic level. To get that, ATALS provides independent models to describe every device property dependence alone, so they can be activated separately. The accuracy of the results obtained depends on the models used in the simulation process. The physical models can be grouped into five classes: mobility, recombination, carrier statistics, impact ionization, and tunneling. To activate the physical model, the MODELS statement is used:

MODELS <model-name>

III.6 Numerical method

In ATLAS there are three different numerical methods that can be used for calculating the solutions to semiconductor device problems:

1. The GUMMEL: will solve for each unknown in turn keeping the other variables constant, repeating the process until a stable solution is achieved.
2. The NEWTON: solve the total system of unknowns together.
3. The BLOCK: will solve some equations fully coupled, while others are de-coupled.

Numerical methods are given in the METHOD statements of the input file with specifying the numerical technique. For example:

METHOD GUMMEL

III.7 Solution specification

Solution specification can be divided up into two types: save, and solve.

- There is two different ways to save in ATLAS according to the type of the solution that will be saved, if device structure that will be stored then the SAVE statement is used, but if the terminal characteristics calculated will be stored, we must use the LOG statement. For example:

  SAVE OUTF=<FILENAME>

  LOG OUTF=<FILENAME>

- There are two different ways to start a solution: use SOLVE statement to start simulation (optical or voltage), or to give the solve initial, and use the LOAD statement if you wish to begin a solution at a previously solved bias point re-load the structure file saved at that point. For example:

  SOLVE INTIN

  LOAD INFILE=<filename> MASTER

III.8 Simulation results and discussions

III.8.1 The simulated structure used in this work

The Simulated structure accredited in our study is shown in figure 3.8 and figure 3.9. It consists of a layer of a specific semiconducting material (silicon, GaAs, and InP) followed by a thin layer of graphene with a thickness of 10 nm deposed on all the surface, followed by another layer on the edge which represents anode from the gold with 0.2 μm as thickness. The cathode is simulated as an ohmic contact in the back surface.

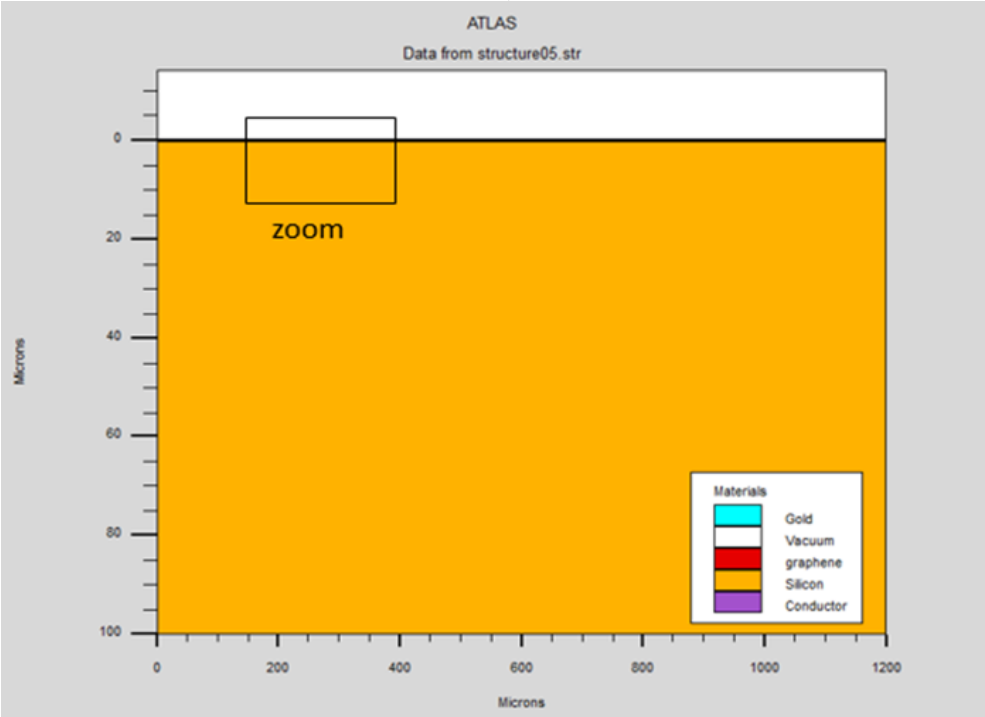

Figure 3.8: simulated structure with silicon as specific material.

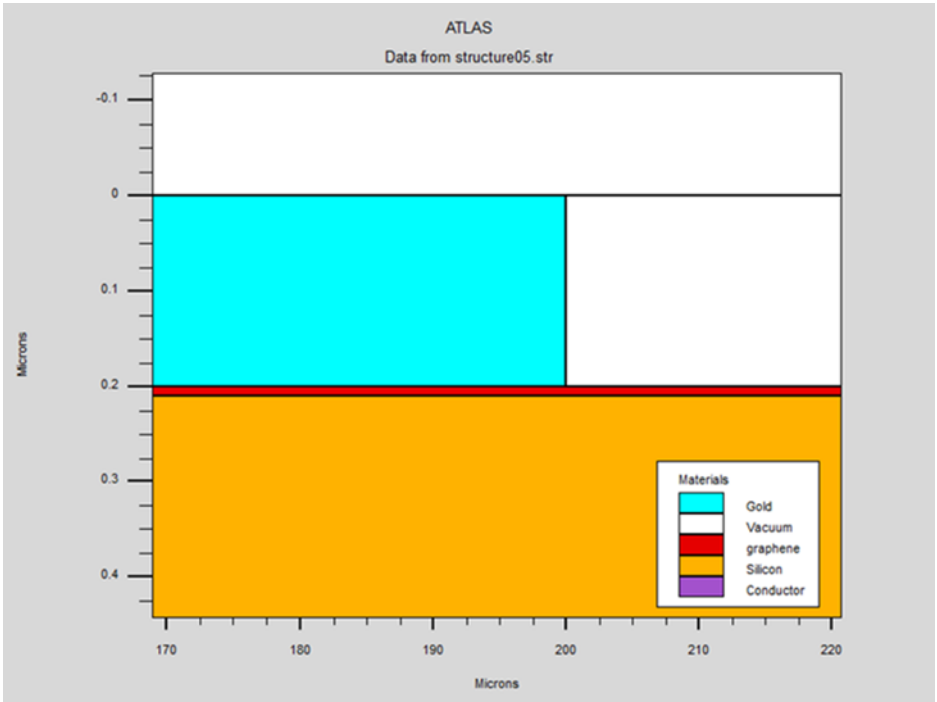

Figure 3.9: zoom of simulated structure with silicon as specific material.

III.8.2 The refractive index file of graphene used in this work

Due to our work on photovoltaic devices, we should define the refractive index file of graphene when specifying material properties in ATLAS. So, the refractive index values of graphene used in the simulation are represented by the graph in figure 3.10:

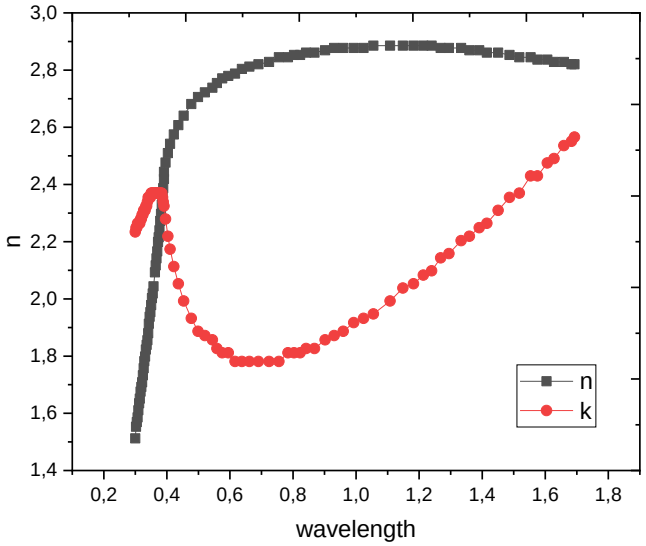

Figure 3.10: real and Imaginary refractive index of grapheme versus optical wavelength [64].

III.8.3 The graphene solar cell simulation

First, we simulated three solar cells using different materials (Si, GaAs, and InP). with the same parameters: 5 (eV) as a work function of graphene, and 1×10^{15} (cm^{-3}) and 100 (μm) as doping and thickness for used material respectively. The simulation results of the three solar cells comparison are shown in figure 3.11 which presents the J-V characteristic, and the output parameters of the solar cells in table 3.1.

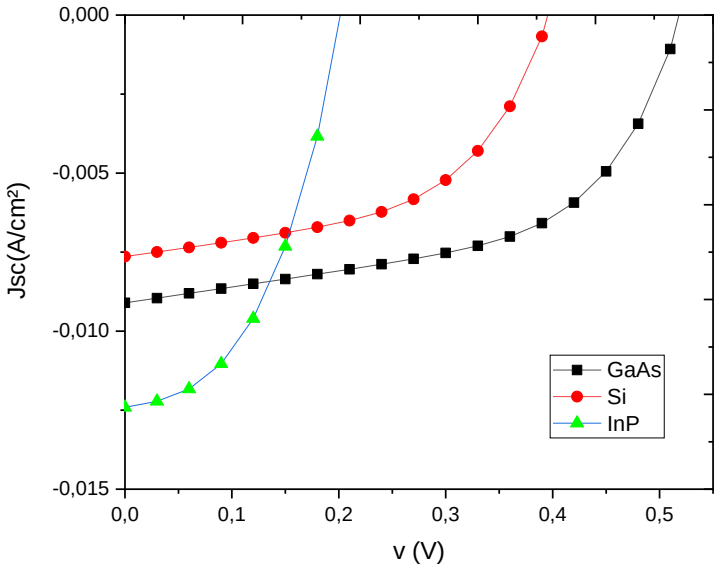

Figure 3.11: comparison J-V characteristic.

Table 3.1: comparison table parameters of the solar cells.

	V_{OC} (V)	$J_{SC}(mA/cm^2)$	FF (%)	η (%)
Si	0.39	7.63	52.07	1.57
GaAs	0.51	9.10	54.41	2.56
InP	0.2	12.4	46.1	1.352

The table shows the different values parameters of the solar cells, we note that the maximal value of V_{OC} is in GaAs cell then Si and finally InP. Also, we notice the same behavior in FF and power conversion efficiency (η). But in J_{SC} we note the maximal value is in InP solar cell then GaAs and Si respectively. The first remark due to the different affinity values for each semiconductor where $\chi_{GaAs} = 4.07$, $\chi_{Si} = 4.1$, and $\chi_{InP} = 4.4$, so Φ_B ($\Phi_{Bn} or\ \Phi_{Bp}$) will have different values according to equation (1.11) that explains the obtained values of V_{OC}. The second remark can be related to the effect of V_{OC} on FF and efficiency (η). Finally, the difference in J_{SC} values can be related to several factors: for silicon and GaAs, the difference is due to space charge region extension which is related to Schottky barrier according to equations (1.11). While the huge short circuit current in case of InP may be due to the extension of the active region which is usually longer in p-type semiconductors than n-type.

III.8.4 The graphene/silicon solar cell simulation

In this part we will study the effect of silicon thickness, graphene thickness, and work function of graphene in Gr/Si Schottky solar cell. The doping used in all studied cells is an n-type doping with density of $10^{15} cm^{-3}$.

III.8.4.1 Effect of silicon thickness on solar cells

We studied the effect of silicon thickness on the J-V characteristic and the solar cell parameters such as open circuit voltage (V_{OC}), fill factor (FF), short circuit current density (J_{SC}), and power conversion efficiency (η). The Si layer thickness is varied from 1 µm to 71 µm while the graphene parameters are fixed at 5 (eV) for work function and 20 (nm) for thickness. The obtained results are shown in figures 3.12 and 3.13.

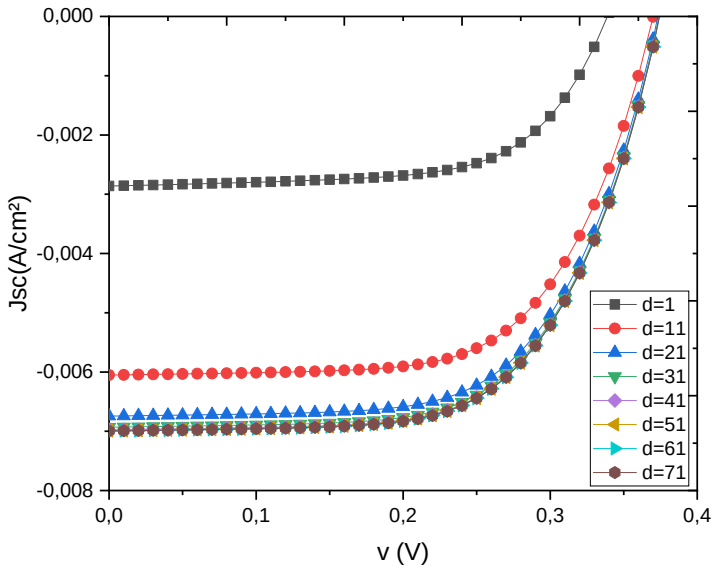

Figure 3.12: effect of silicon thickness on J-V characteristic.

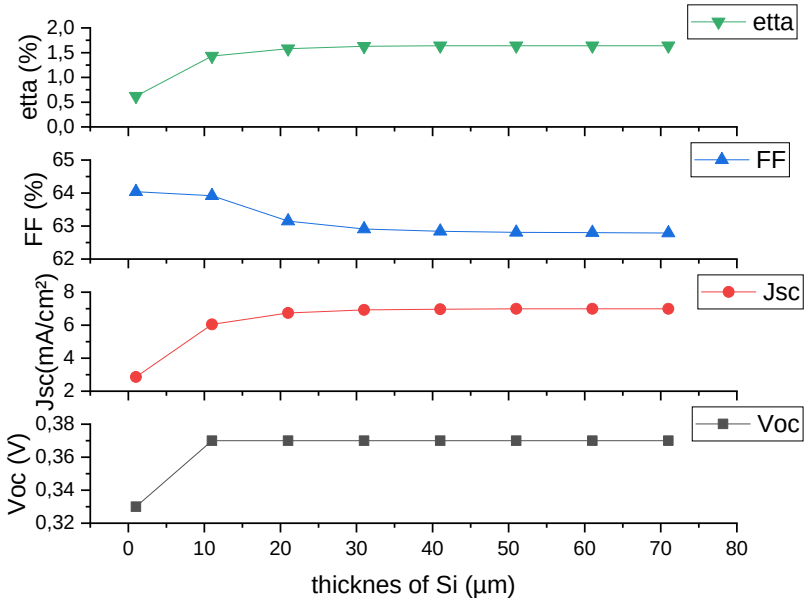

Figure 3.13: effect of silicon thickness on the solar cell parameters.

it can be seen that J_{SC} increases with increasing silicon layer thickness at the beginning after that it will saturate at 6.99 mA/cm². In general, the increase in thickness leads to an increase in the absorption of photons with long wavelengths. But this feature is limited by the ability of the material to absorb these photons. Therefore, the benefit from the increase in

thickness is limited, which leads to saturation of J_{SC}. The same behavior can be seen for the open circuit voltage (which have a direct relationship with J_{SC} according to equation (1.10)) and efficiency. Contrariwise, the fill factor (FF), firstly decreases, then saturates this is because of the change in J_{SC} and V_{OC}.

III.8.4.2 Effect of graphene thickness on solar cells

We studied the effect of graphene thickness on the J-V characteristic and the solar cell parameters such as open circuit voltage (V_{OC}), fill factor (FF), short circuit current density (J_{SC}), and power conversion efficiency (ɳ). The graphene layer thickness is varied from 10 nm to 50 nm, while the value of graphene work function is held at 5 (eV) and a value of silicon thickness at 40 (µm). The obtained results are shown in figures 3.14 and 3.15.

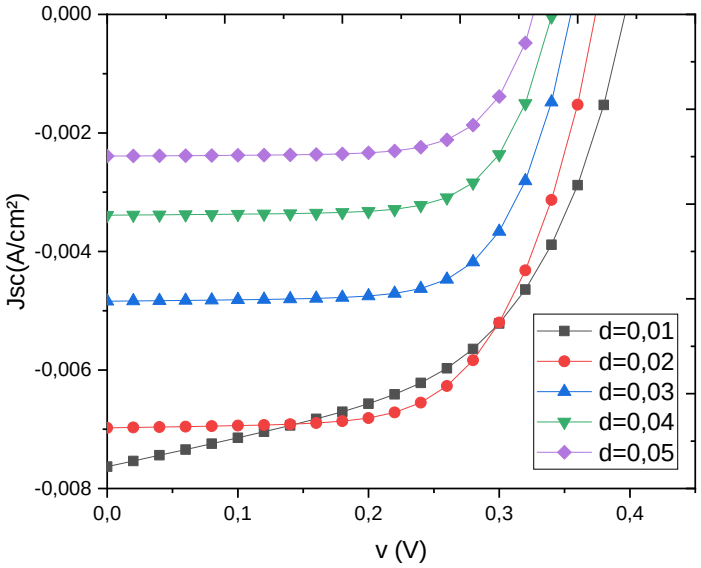

Figure 3.14: effect of graphene thickness J-V characteristic

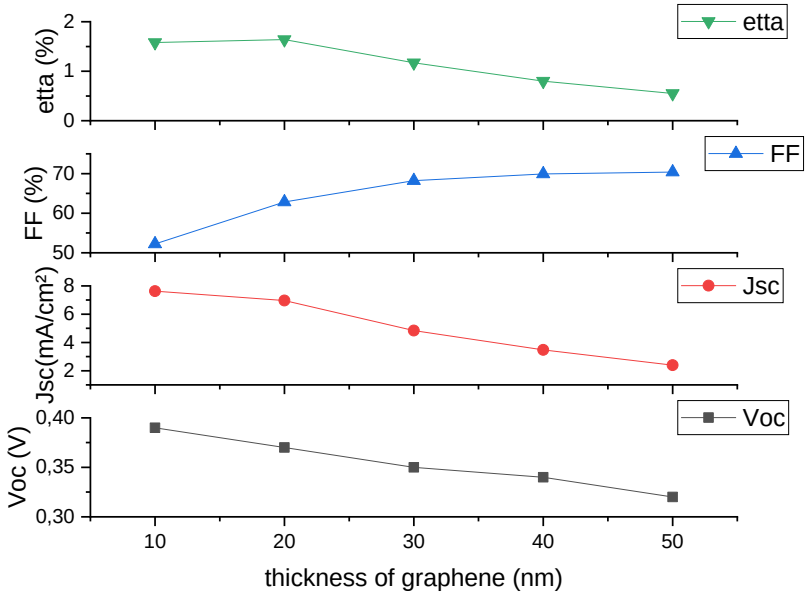

Figure 3.15: effect of graphene thickness on the silicon solar cell parameters.

we note a remarkable decrease in J_{SC}, which can be attributed mainly to two reasons: the active region distance from the surface and the graphene layer transparency. The same behavior can be seen for open circuit voltage which have a direct relationship with short circuit current according to equation (1.9). On the other hand, the fill factor (FF) increases with increasing thickness, which may be explained by the decrease in series resistance due to the increase in cross section. Finally, the efficiency increases slightly at the beginning due to the huge increase in (FF), after that the decrease in J_{SC} and V_{OC} will be the most influential factor.

III.8.4.3 Effect of graphene work function on solar cells

We studied the effect of graphene work function on the J-V characteristic and the solar cell parameters such as open circuit voltage (V_{OC}), fill factor (FF), short circuit current density (J_{SC}), and power conversion efficiency (η). The work function is varied from 4.3 to 5 (eV) [65, 66], while the silicon and graphene thicknesses are held at the values that give the best efficiency which are 40 (µm) and 20 (nm) respectively. The obtained results are shown in figures 3.16 and 3.17.

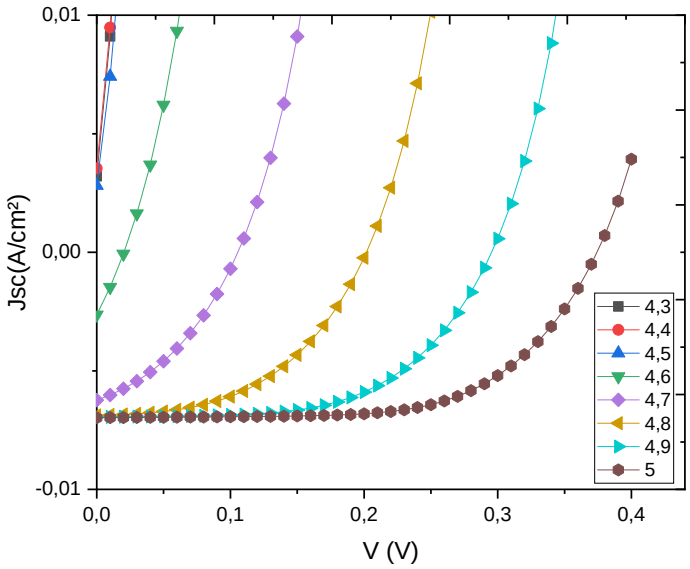

Figure 3.16: effect of graphene work function on J-V characteristic.

It is clear from the JV curves that the cells with graphene work function from 4.3 to 4.5 eV give a positive value of J_{SC} which is the case of Ohmic contact. Therefore, the graphene work function effect will be studied from 4.6 to 5.0 eV, as shown in figure 3.17

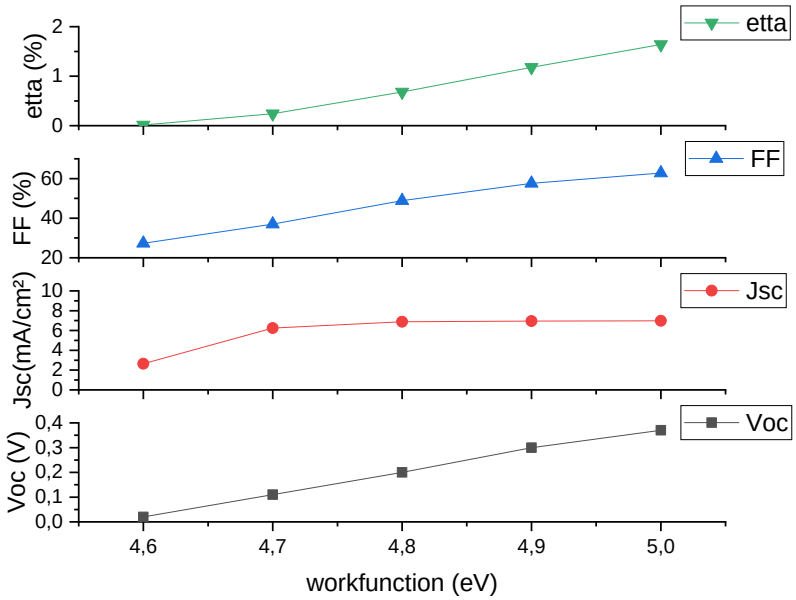

Figure 3.17: effect of graphene work function on the silicon solar cell parameters.

We can note an increase in V_{OC} and FF, the first one can be explained by the increase of Φ_{Bn} according to equation (1.12), while the second (FF) increases due to the decrease of saturation current density according to equation (1.10). As for J_{SC}, we notice an increase which is due to the extension of the depletion region according to equation (1.7). the improvement of V_{OC} and FF and J_{SC} leads to an increase in efficiency (ɳ).

III.8.5 The graphene/GaAs solar cell simulation

In this part we will study the effect of GaAs thickness, graphene thickness, and work function of graphene in Schottky solar cell. The doping used in all studied cells is an n-type doping with density of $10^{15} cm^{-3}$.

III.8.5.1 Effect of GaAs thickness on solar cells

We studied the effect of GaAs thickness on the J-V characteristic and the solar cell parameters such as open circuit voltage (V_{OC}), fill factor (FF), short circuit current density (J_{SC}), and power conversion efficiency (ɳ). The GaAs layer thickness is varied from 0.1 to 50.1 (µm) with set value of graphene work function at 5 (eV) and a value of graphene thickness at 20 (nm). The obtained results are shown in figures 3.18 and 3.19.

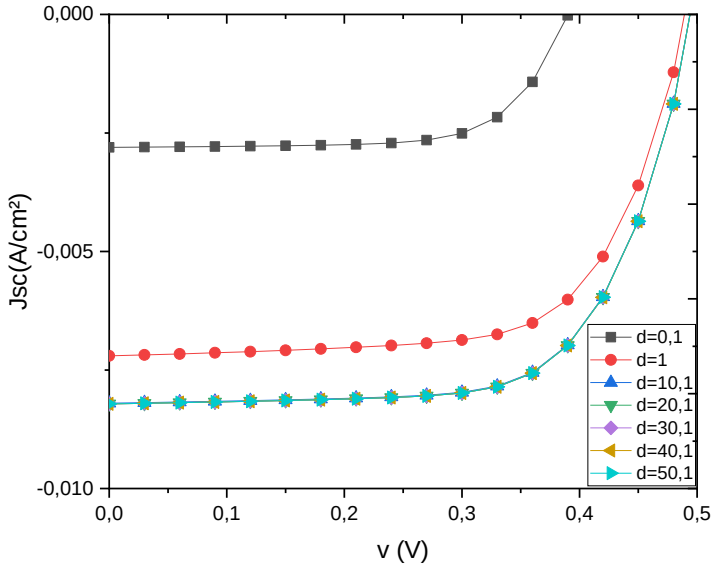

Figure 3.18: effect of GaAs thickness on J-V characteristic.

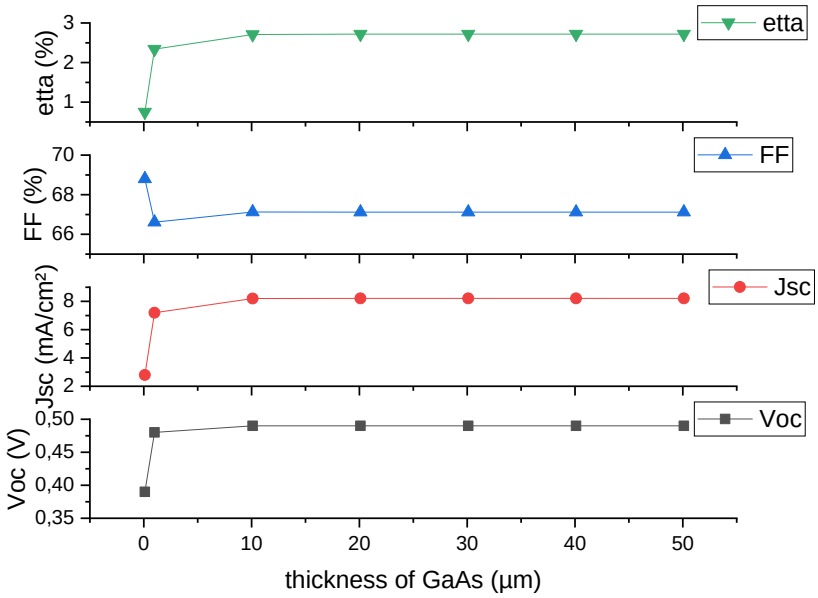

Figure 3.19: effect of GaAs thickness on the solar cell parameters.

The graphs show the different values parameters in GaAs solar cell with changes in GaAs thickness, we note the same remarks for the output parameters J_{SC}, V_{OC}, FF, and η in silicon solar cell with changes in silicon thickness. Where the J_{SC} increases with increasing thickness due to the absorption of long wave length photons, which affects V_{OC} and efficiency (η), while FF decreases then saturates this is because the change in J_{SC} and V_{OC}.

III.8.5.2 Effect of graphene thickness on solar cells

We studied the effect of graphene thickness on the J-V characteristic and the solar cell parameters such as open circuit voltage (V_{OC}), fill factor (FF), short circuit current density (J_{Sc}), and power conversion efficiency (η). The graphene layer thickness is varied from 10 nm to 50 nm, meanwhile its work function is held at 5 (eV) and a value of GaAs thickness at 10 (µm). The obtained results are shown in figures 3.20 and 3.21.

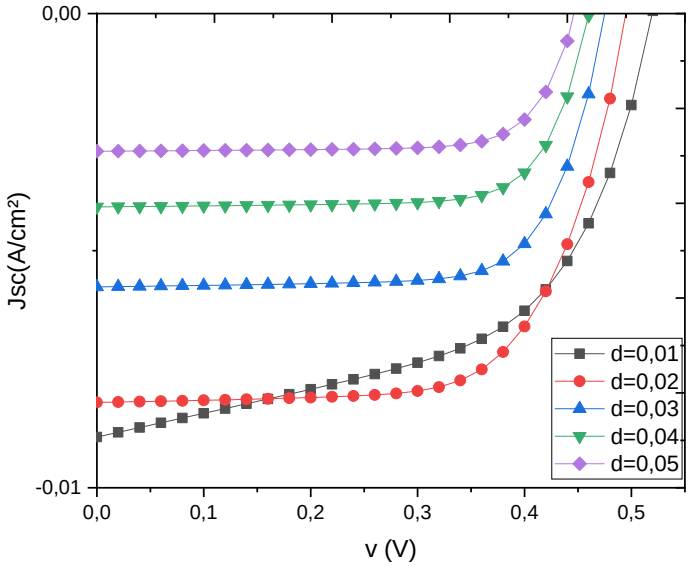

Figure 3.20: effect of graphene thickness on J-V characteristic.

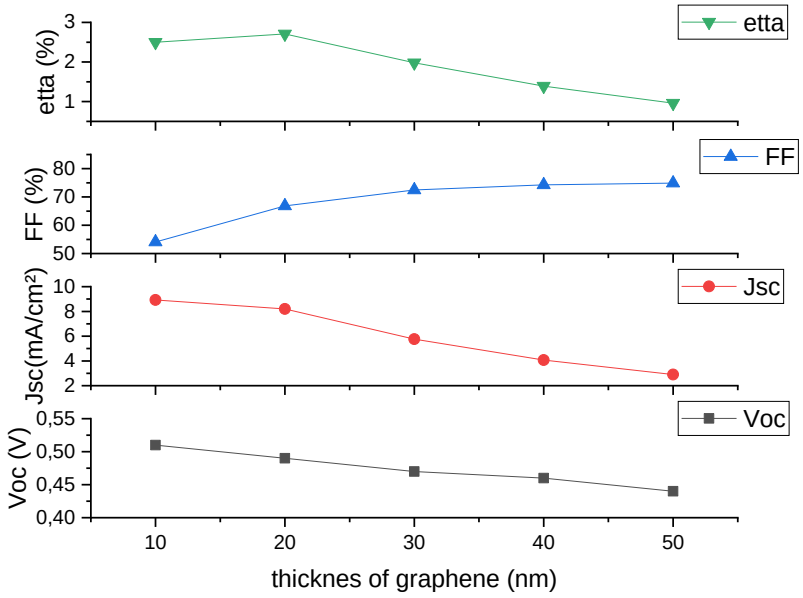

Figure 3.21: effect of graphene thickness on the GaAs solar cell parameters.

The graphs show the different values parameters in silicon solar cell with changes in GaAs thickness, we note the same remarks for the output parameters J_{SC}, V_{OC}, FF, and η in silicon solar cell with changes in silicon thickness.

III.8.5.3 Effect of graphene work function on solar cells

We studied the effect of graphene work function on the J-V characteristic and the solar cell parameters such as open circuit voltage (V_{OC}), fill factor (FF), short circuit current

density (J_{sc}), and power conversion efficiency (η). The work function is varied from 4.3 to 5 (eV) with set value of GaAs thickness at 10 (µm) and a value of graphene thickness at 20 (nm). The obtained results are shown in figures 3.22 and 3.23.

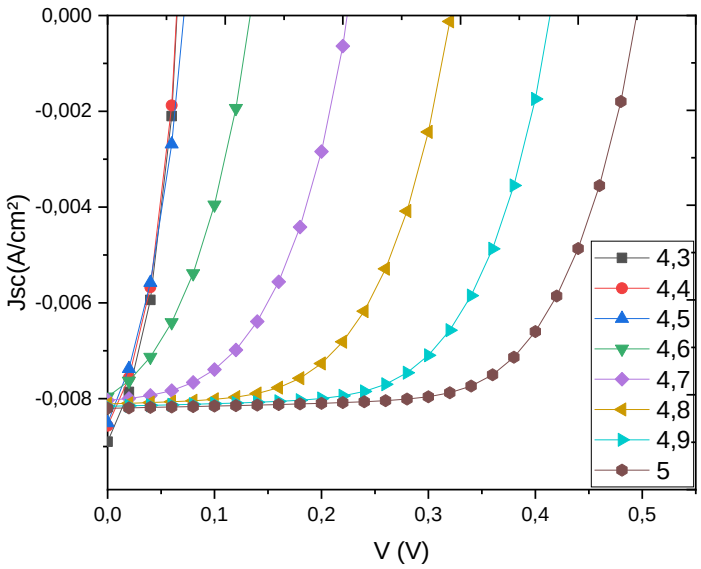

Figure 3.22: effect of graphene work function on J-V characteristic.

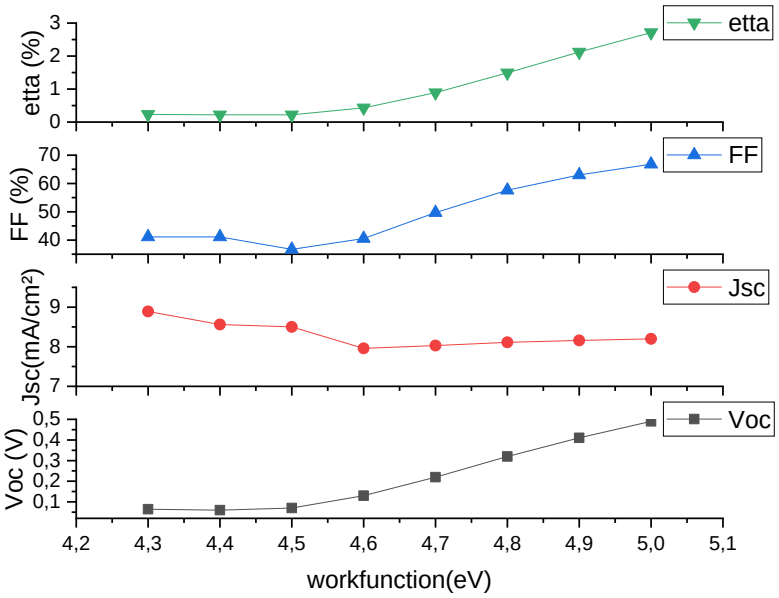

Figure 3.23: effect of graphene work function on the GaAs solar cell parameters.

The graphs show the variation of GaAs solar cell output parameters a function of graphene work function, we note an increase in V_{OC} that can be explained by the increase of Φ_{Bn} according to equation (1.12). While, the short circuit current shows a strange behavior at the beginning (4.3-4.6 eV), then it increases due to the extension of the depletion region according to equation (1.7). On the other hand, the increase of FF can be related to the increase of the saturation current which has a direct relation with Φ_{Bn} as shown in equation (1.11). Finally, all the above affect the power conversion efficiency which increases with increasing work function

III.8.6 The graphene/InP solar cell simulation

In this part we will study the effects of InP thickness, graphene thickness, and work function of graphene in Schottky solar cell. The doping used in all studied cells is an p-type doping with density of $10^{15} cm^{-3}$.

III.8.6.1 Effect of InP thickness on solar cells

We studied the effect of InP thickness on the J-V characteristic and the solar cell parameters such as open circuit voltage (V_{OC}), fill factor (FF), short circuit current density (J_{Sc}), and power conversion efficiency (η). The InP layer thickness is varied from 0.1 to 100 (µm) with set value of graphene work function at 5 (eV) and a value of graphene thickness at 10 (nm). The obtained results are shown in figures 3.24 and 3.25.

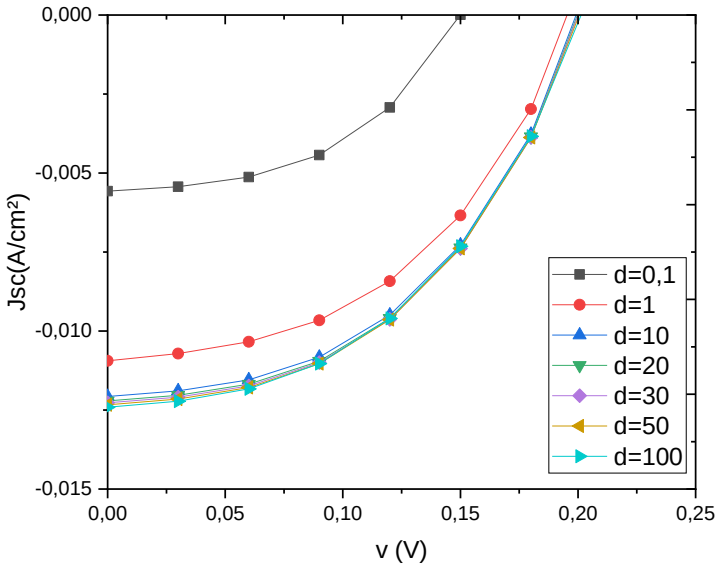

Figure 3.24: effect of InP thickness on J-V characteristic.

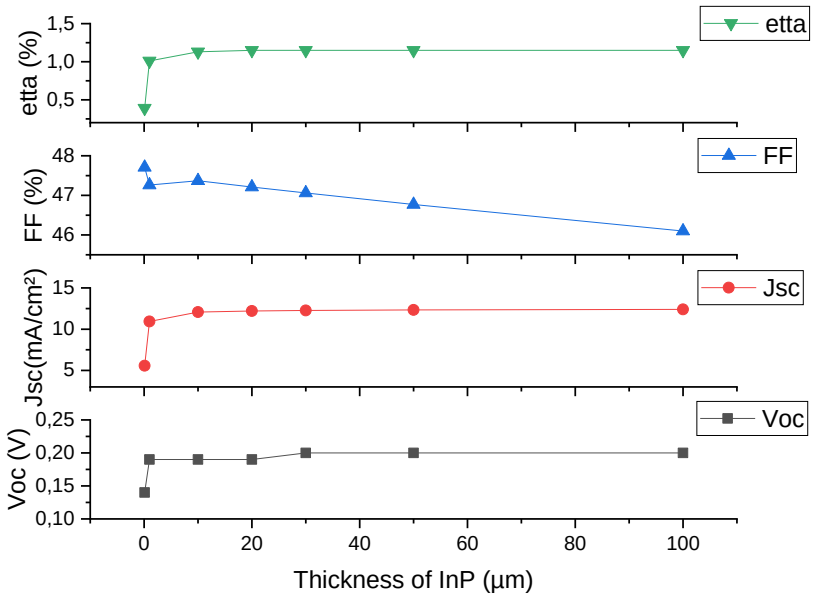

Figure 3.25: effect of InP thickness on the solar cell parameters.

The graphs show the different values parameters in InP solar cell with changes in InP thickness, we note the same remarks for the output parameters J_{SC}, V_{OC}, η, and FF in silicon solar cell with changes in silicon thickness. So, the same previous interpretations are correct in this case**.**

III.8.6.2 Effect of graphene thickness on solar cells

We studied the effect of graphene thickness on the J-V characteristic and the solar cell parameters such as open circuit voltage (V_{Oc}), fill factor (FF), short circuit current density (J_{Sc}), and power conversion efficiency (η). The graphene layer thickness is varied from 10 nm to 50 nm with set value of graphene work function at 4.3 (eV) and a value of InP thickness at 30 (µm). The obtained results are shown in figures 3.20 and 3.21.

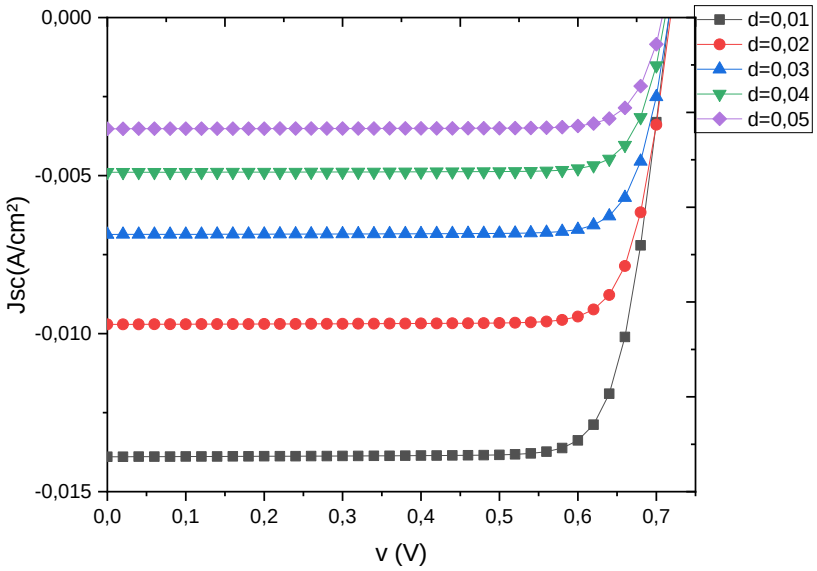

Figure 3.26: effect of graphene thickness on J-V characteristic.

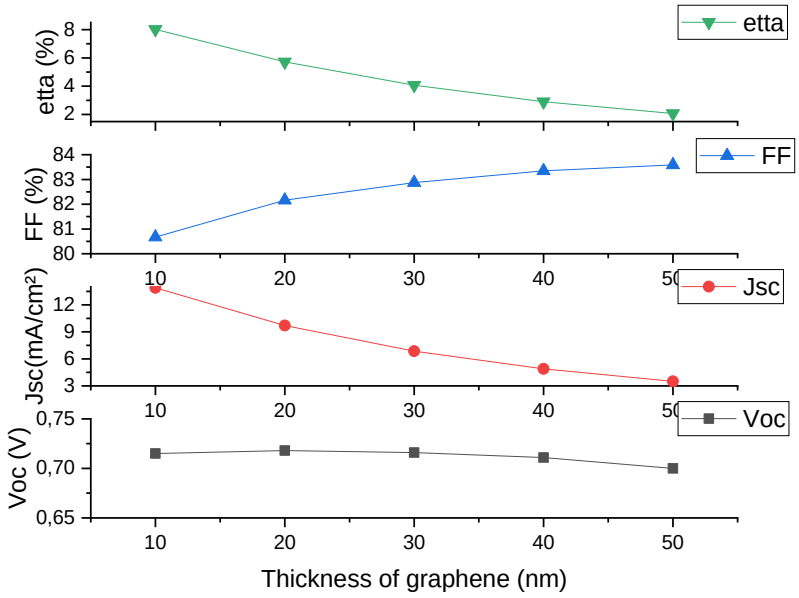

Figure 3.27: effect of graphene thickness on the InP solar cell parameters.

The graphs show the different values parameters in InP solar cell with changes in graphene thickness, we note the same remarks for the output parameters J_{SC}, V_{OC}, η, and FF in silicon solar cell with changes in silicon thickness. In this case, we depend on the same the previous interpretation.

III.8.6.3 Effect of graphene work function on solar cells

We studied the effect of graphene work function on the J-V characteristic and the solar cell parameters such as open circuit voltage (V_{OC}), fill factor (FF), short circuit current density (J_{SC}), and power conversion efficiency (η). The work function is varied from 4.3 to 5 (eV) with set value of InP thickness at 30 (µm) and a value of graphene thickness at 10 (nm). The obtained results are shown in figures 3.28 and 3.29.

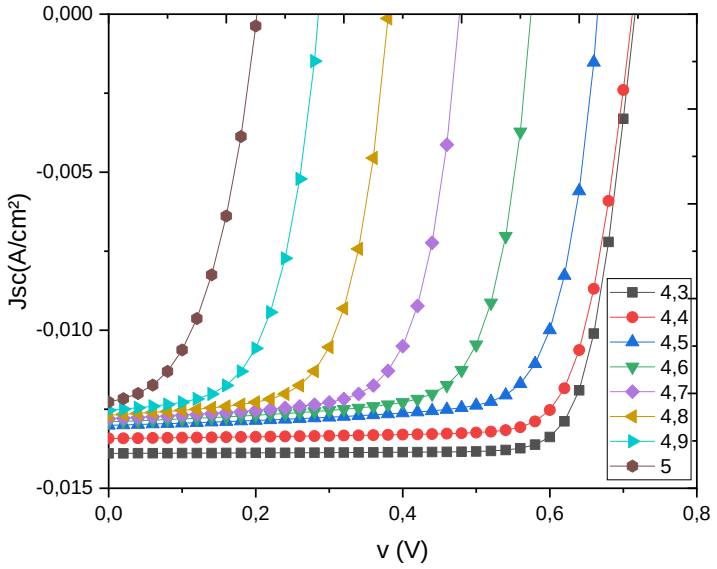

Figure 3.28: effect of graphene work function on J-V characteristic.

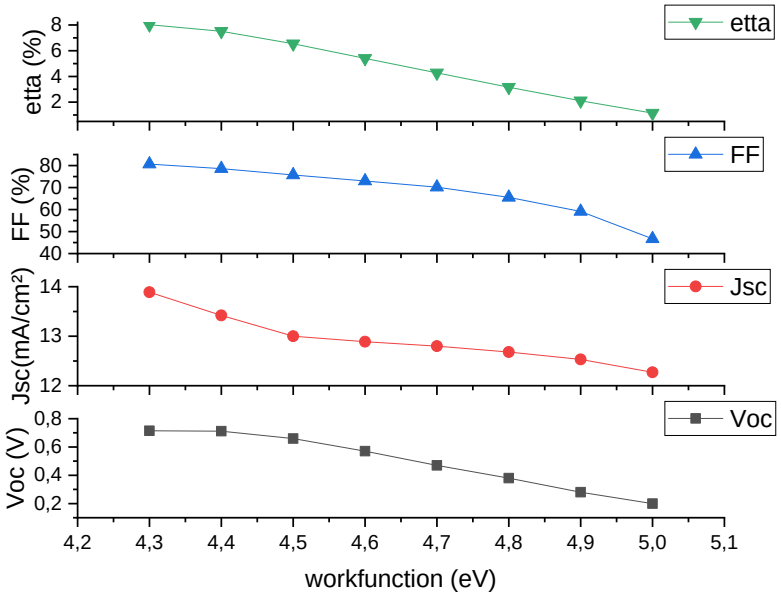

Figure 3.29: effect of graphene work function on the InP solar cell parameters.

In InP solar cell we note the opposite behavior in output parameters (J_{SC}, V_{OC}, FF, and η) compared to silicon output parameters solar cell, this is due to the different type of doping used. Where we remark: decrease in all the parameters. This can be related mainly to the barrier behavior which in p-type semiconductors decreases with increasing graphene work function according to equation (1.5).

Conclusion

Conclusion

In this work, we compared the performance of different graphene-based heterojunction solar cells, in three different materials and tried to optimize their performance by studying some effects (such as thickness, work function ...etc.) by simulation using the Silvaco Atlas software.

In the same condition, the simulation showed best efficiency in GaAs solar cells (2.56%), however, in silicon (1.57%) and InP (1.35%).

The second study can be divided into three parts, in each part we optimized each solar cell separately: silicon, GaAs, and InP respectively. We found:

- In silicon solar cell, we obtained maximum efficiency (1.64%) in following condition: Si thickness (40 µm), graphene thickness (20 nm), and graphene work function (5 eV).
- In GaAs solar cell, we obtained maximum efficiency (2.71%) in following condition: GaAs thickness (10 µm), graphene thickness (20 nm), and graphene work function (5eV).
- In InP solar cell, we obtained maximum efficiency (8.02%) in following condition: InP thickness (30 µm), graphene thickness (10 nm), and graphene work function (4.3eV).

.

References

1. Hansen, J., et al., *Assessing "dangerous climate change": Required reduction of carbon emissions to protect young people, future generations and nature.* PloS one, 2013. **8**(12): p. e81648.
2. *World Energy & Climate Statistics – Yearbook 2022* [cited 2023; Available from: https://yearbook.enerdata.net/total-energy/world-consumption-statistics.html.
3. *years of fossil fuel reserves left, 2020*. [cited 2023; Available from: https://ourworldindata.org/grapher/years-of-fossil-fuel-reserves-left.
4. *Electricity from renewable sources on the rise*. [cited 2023; Available from: https://ec.europa.eu/eurostat/web/products-eurostat-news/w/DDN-20230127-1.
5. Jayawardena, K.I., et al., *'Inorganics-in-Organics': recent developments and outlook for 4G polymer solar cells.* Nanoscale, 2013. **5**(18): p. 8411-8427.
6. ABD EL OUADOUD, S.A., *Study of Silicon-Graphene solar cells by Simulation.*
7. Kaouther, C., *Study of graphene-based solar cells by simulation.*
8. Lemons, D.S., W.R. Shanahan, and L.J. Buchholtz, *On the Trail of Blackbody Radiation: Max Planck and the Physics of his Era*2022: MIT Press.
9. Corkish, R., et al., *Applied Photovoltaics*2007: Earthscan.
10. Wenham, S.R., et al., *Applied Photovoltaics*2013: Taylor & Francis.
11. Kita, T., Y. Harada, and S. Asahi, *Energy Conversion Efficiency of Solar Cells*2019: Springer Singapore.
12. Bose, B.K., *Power Electronics in Renewable Energy Systems and Smart Grid: Technology and Applications*2019: Wiley.
13. Smestad, G.P., *Optoelectronics of Solar Cells*2002: Society of Photo Optical.
14. Kalogirou, S.A., *Solar Energy Engineering: Processes and Systems*2009: Elsevier Science.
15. Sze, S.M. and M.K. Lee, *Semiconductor Devices: Physics and Technology*2012: Wiley.
16. Barlow, M.D., *Metal-semiconductor contacts for schottky diode fabrication*, 2007.
17. Mathieu, H. and H. Fanet, *Physique des semiconducteurs et des composants électroniques - 6ème édition: Cours et exercices corrigés*2009: Dunod.
18. Markvart, T. and L. Castañer, *Chapter I-1-A - Principles of Solar Cell Operation*, in *McEvoy's Handbook of Photovoltaics (Third Edition)*, S.A. Kalogirou, Editor 2018, Academic Press. p. 3-28.
19. *solar cell structure*. [cited 2023; Available from: https://www.pveducation.org/pvcdrom/solar-cell-operation/solar-cell-structure.
20. Mishra, U. and J. Singh, *Semiconductor Device Physics and Design*2007: Springer Netherlands.
21. Mertens, K., *Photovoltaics: Fundamentals, Technology, and Practice*2018: Wiley.
22. Sze, S.M. and K.K. Ng, *Physics of Semiconductor Devices*2006: Wiley.
23. Markvart, T. and L. Castaner, *Solar Cells: Materials, Manufacture and Operation*2004: Elsevier Science.
24. Yang, W., et al., *Internal quantum efficiency for solar cells.* Solar Energy, 2008. **82**(2): p. 106-110.
25. Ananda, W. *External quantum efficiency measurement of solar cell*. in *2017 15th International Conference on Quality in Research (QiR): International Symposium on Electrical and Computer Engineering*. 2017. IEEE.
26. Dennler, G., et al., *Angle dependence of external and internal quantum efficiencies in bulk-heterojunction organic solar cells.* Journal of Applied Physics, 2007. **102**(5): p. 054516.
27. Green, M., et al., *Solar cell efficiency tables (version 57).* Progress in photovoltaics: research and applications, 2021. **29**(1): p. 3-15.
28. Handy, R., *Theoretical analysis of the series resistance of a solar cell.* Solid-State Electronics, 1967. **10**(8): p. 765-775.
29. Araujo, G.L. and E. Sanchez, *A new method for experimental determination of the series resistance of a solar cell.* IEEE Transactions on Electron Devices, 1982. **29**(10): p. 1511-1513.

30. Dhass, A., E. Natarajan, and L. Ponnusamy. *Influence of shunt resistance on the performance of solar photovoltaic cell*. in *2012 International conference on emerging trends in electrical engineering and energy management (ICETEEEM)*. 2012. IEEE.
31. Et-taya, L., T. Ouslimane, and A. Benami, *Numerical analysis of earth-abundant Cu2ZnSn (SxSe1-x) 4 solar cells based on Spectroscopic Ellipsometry results by using SCAPS-1D.* Solar Energy, 2020. **201**: p. 827-835.
32. Bagher, A.M., M.M.A. Vahid, and M. Mohsen, *Types of solar cells and application.* American Journal of optics and Photonics, 2015. **3**(5): p. 94-113.
33. Munzer, K.A., et al., *Thin monocrystalline silicon solar cells.* IEEE Transactions on Electron Devices, 1999. **46**(10): p. 2055-2061.
34. Kalogirou, S.A., *Chapter nine - Photovoltaic Systems*, in *Solar Energy Engineering*, S.A. Kalogirou, Editor 2009, Academic Press: Boston. p. 469-519.
35. Sherwani, A.F., J.A. Usmani, and Varun, *Life cycle assessment of solar PV based electricity generation systems: A review.* Renewable and Sustainable Energy Reviews, 2010. **14**(1): p. 540-544.
36. Koch, C., M. Ito, and M. Schubert, *Low-temperature deposition of amorphous silicon solar cells.* Solar Energy Materials and Solar Cells, 2001. **68**(2): p. 227-236.
37. Gloeckler, M., I. Sankin, and Z. Zhao, *CdTe solar cells at the threshold to 20% efficiency.* IEEE Journal of Photovoltaics, 2013. **3**(4): p. 1389-1393.
38. Suhaimi, S., et al., *Materials for enhanced dye-sensitized solar cell performance: Electrochemical application.* Int. J. Electrochem. Sci, 2015. **10**(4): p. 2859-2871.
39. Wang, D., et al., *Stability of perovskite solar cells.* Solar Energy Materials and Solar Cells, 2016. **147**: p. 255-275.
40. Díez-Pascual, A.M., et al., *Recent developments in graphene/polymer nanocomposites for application in polymer solar cells.* Polymers, 2018. **10**(2): p. 217.
41. *Best Research-Cell Efficiency Chart*. [cited 2023; Available from: https://www.nrel.gov/pv/cell-efficiency.html.
42. Enoki, T. and T. Ando, *Physics and Chemistry of Graphene: Graphene to Nanographene*2013: Jenny Stanford Publishing.
43. Harun, S.W., *Handbook of graphene. Volume 7, Biomaterials*, 2019, Scrivener Publishing: Beverly, MA.
44. Choi, W. and J. Lee, *Graphene: Synthesis and Applications*2016: CRC Press.
45. Gong, J.R., *Graphene: Synthesis, Characterization, Properties and Applications*2011: IntechOpen.
46. Novoselov, K., et al., *Electronic properties of graphene.* phys. stat. sol.(b), 2007. **244**(11): p. 4106-4111.
47. Al-Ahmed, A., *Graphene from Natural Sources: Synthesis, Characterization, and Applications*2022: CRC Press.
48. Yin, Z., et al., *Graphene-Based Materials for Solar Cell Applications.* 2013.
49. Basu, S., *Crystalline Silicon: Properties and Uses*2011: IntechOpen.
50. Tilli, M., et al., *Handbook of Silicon Based MEMS Materials and Technologies*2009: Elsevier Science.
51. Hull, R. and INSPEC, *Properties of Crystalline Silicon*1999: INSPEC.
52. Weerasinghe, H.C., *Electrical characterization of metal-to-insulator transition in iron silicide thin films on sillicone substrates*, 2006, University of South Florida.
53. *periodic table*. [cited 2023; Available from: https://www.snexplores.org/article/scientists-say-periodic-table.
54. Li, X., et al., *Graphene-on-silicon Schottky junction solar cells.* Advanced materials, 2010. **22**(25): p. 2743-2748.
55. Yang, L., et al., *Interface engineering for efficient and stable chemical-doping-free graphene-on-silicon solar cells by introducing a graphene oxide interlayer.* Journal of Materials Chemistry A, 2014. **2**(40): p. 16877-16883.

56. Nasir, H.N., H.M. Abduljalil, and M.A. Abdulsattar, *Study The Effect Of Sulfur Atoms On The Electronic Structure For The Gallium Arsenide Nanocrystals Of Eight Atoms.* Journal of University of Babylon, 2013. **21**(5).
57. Shur, M.S., *GaAs Devices and Circuits*2013: Springer US.
58. Tridane, M., A. Malaoui, and S. Belaaouad, *Numerical Simulation of pin GaAs Photovoltaic Cell Using SCAPS-1D.* 2022.
59. Yu, M., et al., *Numerical simulation of graphene/GaAs heterojunction solar cells.* Solar Energy, 2019. **182**: p. 453-461.
60. Jie, W., F. Zheng, and J. Hao, *Graphene/gallium arsenide-based Schottky junction solar cells.* Applied physics letters, 2013. **103**(23): p. 233111.
61. Manasreh, M.O., *InP and Related Compounds: Materials, Applications and Devices*2000: Taylor & Francis.
62. Israel, S., R. Saravanan, and R. Rajaram, *Electronic structure of InP at RT, 200 and 100 K.* Physica B: Condensed Matter, 2004. **349**(1-4): p. 390-400.
63. Wang, P., et al., *Tunable graphene/indium phosphide heterostructure solar cells.* Nano Energy, 2015. **13**: p. 509-517.
64. Yang, Y., et al., *Invited Article: Enhanced four-wave mixing in waveguides integrated with graphene oxide.* APL Photonics, 2018. **3**(12): p. 120803.
65. Arefinia, Z. and A. Asgari. *Modeling of the graphene based Schottky barrier solar cells on InGaN substrate*. in *2014 22nd Iranian Conference on Electrical Engineering (ICEE)*. 2014. IEEE.
66. Akada, K., et al., *Control of work function of graphene by plasma assisted nitrogen doping.* Applied physics letters, 2014. **104**(13): p. 131602.